GENETIC ENGINEERING OF PROTEINS FOR BIOTECHNOLOGY APPLICATIONS

by

YANBO ZHANG

Presented to the Faculty of the Graduate School of

The University of Texas at Arlington in Partial Fulfillment

of the Requirements

for the Degree of

DOCTOR OF PHILOSOPHY

THE UNIVERSITY OF TEXAS AT ARLINGTON

DECEMBER 2013

Acknowledgements

Five memorable years was dedicated from the Aug of 2009 to the Dec of 2013 to studying and learning chemistry. Standing at this last step before completion my degree, I wish to convey my gratitude to everyone at the Department of Chemistry and University of Texas at Arlington for making this possible.

In particular, I wish to give my most cordial thanks and appreciation to my advisor, Dr. Roshan Perera, for his inspiring ideas, timely advice, and whole hearted support which provided me with the motivation to work on challenging projects and later led to the successful completion of all my projects.

I would also thank my committee members, Dr. Frederick M. Macdonnell and Dr. Subhrangsu S. Mandal for their generous, invaluable guidance and support throughout these years.

I would like to acknowledge the academic support provided by the faculty and staff members at the Chemistry department.

It has been a great pleasure to meet and work with all the Perera lab associates and appreciate their valuable helps.

I am heartily indebted to my parents for their love, their unconditional support and to my brother, my grandma for their motivation and their love.

Finally, I offer my gratitude to the University of Texas at Arlington for giving me this opportunity to finish my doctoral degree here in Arlington, Texas.

November 27, 2013

Abstract

GENETIC ENGINEERING OF PROTEINS FOR BIOTECHNOLOGY APPLICATIONS

Yanbo Zhang, PhD

The University of Texas at Arlington, 2013

Supervising Professor: Roshan Perera

Heme *b* (protoporphyrin IX or protoheme) plays a major role in the structure and function in proteins such as myoglobin (Mb), hemoglobin (Hb), horseradish peroxidase (HRP), catalase, cytochrome P450 as well as catalase peroxidase (KatG). This highly conjugated porphyrin system forms the cradle for the iron containing prosthetic group of the hemeproteins. Although the surrounding chiral protein scaffold is important in protein reactivity and selectivity, the heme iron prosthetic group creates a focal point for the substrate reactivity.

The genetic incorporation of unnatural amino acids (UAA) into proteins *in vivo,* using the same biosynthetic machinery used by living cells to synthesize proteins, has proven a powerful technique for investigating structure and function of proteins. An orthogonal tRNA/aminoacyl-tRNA synthetase pair allows selective and efficient incorporation of unnatural amino acids into proteins *in vivo* at sites specified by the amber nonsense codon, TAG. These include redox-active amino acids, metal-binding amino acids, fluorescent and infrared probes, photo- and chemically reactive amino acids and post-translationally modified amino acids. Therefore, this method potentially paves the way for the design of proteins that display enhanced or unique functionality. Furthermore, this novel biotechnological tool produces native conformation of proteins with high yields at low cost. Contrary to this, the total synthesis of proteins with UAA using solid-phase

synthesis is much more complicated due to size limitations (~60-100 amino acids) as well as producing denatured proteins at a very low yield. We will be examining two important heme protein targets, KatG, Mb, and enhanced green fluorescence protein (EGFP) to uncover their structural and functional secrets using this biotechnological tool. The overall goal of this research is to establish an experimental framework that enables the site-specific incorporation of unnatural amino acids into various recognized sites in these proteins targets, to study the functional secrets in these proteins, and to construct biopolymer mimics for industrial applications. Three factors control the functional properties of these enzymes: (i) the coordination state of the iron complex; (ii) the nature of the axial ligands in the fifth and sixth coordination sites; and (iii) the protein active site heme environment including the polarity of the surroundings and the accessibility of substrates and solvents to the metal.

Preface

Three broad specific aims will be addressed in order to advance our understanding in the generation, characterization, and most importantly their biotechnological use. These primary aims will be achieved by site-specific incorporation of unnatural amino acids, dihydroxyphenylalanine (DOPA) and 3-aminotyrosine (3-NH_2Tyr) into KatG, EGFP and sperm whale Mb. Therefore, the following aims will be pursued:

The KatG isolated from *Francisella tularensis* was my focal study in first three chapters in this thesis. This bifunctional enzyme is the least characterized out of all the catalase peroxidases. Therefore, still the exact nature of the active species responsible for the peroxide activation to carry out catalase as well as peroxidase functions are not known. Researchers continue to ask fundamental questions; how does the KatG activate peroxidases? How can the KatG perform two vastly different reactions, hydrogen peroxide decomposition and peroxidase substrate reduction, using the same prosthetic heme? What factors govern this transformation within protein environment? Can we effectively model the heme protein active site using a natural probe like sperm whale Mb? To remove some ambiguity and to find answers for some of these questions, a comprehensive attempt has been made to investigate the structure and reactivity of the KatG in this thesis. This wide scope approach includes cloning, expression, characterization, kinetic studies and investigations of the mechanism of catalysis. The central theme of my research is to understand the structural and functional properties of KatG and to develop new biotechnological applications. We have successfully carried out these aims for KatG as shown in this thesis.

EGFP has been used for sometime in the protein labeling and *in vivo* cellular imaging work for sometime now. There are many reports on expansion of the physical properties of the color fluorophore within this protein. However, our attempt is to use unnatural amino acids, DOPA and 3-NH2Tyr and expand the limits of the color spectrum of this protein. WE have successfully generated two reddish colors in this work as described in chapter 4.

Recently, the His93Gly (H93G) “cavity” mutant of myoglobin has been used as a versatile scaffold for modeling heme states. The ability in accessibility of the proximal cavity with different ligands led to prepare mixed ligand adducts, in ferrous, ferric as well as ferryl oxidation states. In addition, it has been possible to prepare complexes that are difficult to generate with synthetic heme models in organic solvents. In the presence of excess amine, for example, ferric porphyrin model systems are reduced to bis(amine)iron(II) complexes. In contrast, our investigation with Mb was to genetically modify it and generate extraordinary artificial protein, such as bismetallo Mb and super functional Mb-Mb dimer protein. Here, we have shown that H48(*p*-iodophenylalnine) Mb can cross couple with H48(*p*-boronophenylalanine) Mb using $Pd(OAc)_2$ as the catalyst (the Suzuki cross-coupling reaction) to generate a larger bioscaffold with two heme centers. Hence this work is unprecedented as the potential to introduce new biocatalysts to the biotechnology field.

Table of Contents

List of Illustrations

List of Tables

Chapter 1

Cloning and Expression of Recombinant Catalase-Peroxidase (KatG) from *Francisella tularensis* with Unnatural Amino Acid

All the experiments in this chapter were done by Yanbo Zhang in the laboratory of Prof. Roshan Perera.

1.1 Introduction

Francisella tularensis is a gram-negative bacterium that can cause tularemia in humans and mammals. Though tularemia in humans are rare, tularemia caused by *Francisella tularensis* subspecies (*holarctica, tularensis, mediasiatica* etc.) are more common in many countries including in North America. Some are extremely infectious, and inhalation of as few as 10 CFU is sufficient to cause disease in humans.[1-2]

Catalase-peroxidase (KatG) from *Mycobacterium tuberculosis* has generated much interest due to its ability to develop isoniazid (the front-line antitubercular agent resistancy).[3-5] Resistance *Mycobacterium tuberculosis* displays mutation in the KatG that alters the function of the enzyme.[6-11] Furthermore, highly virulent pathogens contain more of unique periplasmic KatG from the non-pathogenic relatives. Therefore, KatG's structural and functional studies are important for drug development process against these pathogens.[2,11-12]

It is known that oxygen-rich environment can be a cause for various degrees of oxidative stress due to reactive oxygen species (ROS) produced as by-product during the endogenous metabolism. Furthermore, H_2O_2 can act as a defensive agent against invading pathogens, by the mammalian host. Pathogens, such as *Francisella tularensis* strains, *SCHU S4* have developed a resistant mechanism using KatG dependent withstand of the antimicrobial effects exerted by hydrogen peroxide (H_2O_2).[13] KatG shows bifunctionality by combining the monofunctionalities exhibited by catalases and peroxidase.[2] KatG active heme center is consisted with a peroxidase conserved proximal Histidine residue, compared to the catalase, which contains a proximal tyrosine residue.[13] Though KatG from *Francisella tularensis* has not been well characterized, KatG proteins preserve in *Mycobacterium tuberculosis* and *Cyanobacterium synechocystis* have been crystallized and studied to some extent.[2,14-16] KatG typically has an extensive hydrogen-

bonding network, more responsible to peroxidase activity, via some conserved amino acids, that is sensitive to mutations.[17-18]

Hence, KatG from *Francisella tularensis* gene was isolated from genomic DNA, cloned into a high expression pBAD plasmid, expressed, and characterized to demonstrate its unique bifunctional capabilities. Additionally, the H_2O_2 kinetics has been thoroughly studied for their slow H_2O_2 decomposition capabilities compound to faster catalase activity rates.

First of all, since the KatG from *Francisella tularensis* has not been fully characterized as well as no crystal structure is available. Therefore, I have carried out a computational molecular modeling to find more about the structure associated with KatG gene (Figure 1-1a and b). This will be useful in locating a residue for the mutation on the surface of KatG for tagging experiments (as shown in Chapter 2). Based on this computer-generated structure, we have identified Tyr559 as the position to incorporate amino acid via site-directed mutagenesis with amber nonsense codon (TAG) to selectively incorporate L-3,4-dihydroxyphenylalanine (DOPA) unnatural amino acid. This will be accomplished by an orthogonal tRNA/aminoacyl-tRNA synthetase pair from *Methanococcus jannaschii* (*Mj*) which allows selective and efficient incorporation of unnatural amino acids into proteins *in vivo* at sites specified by the TAG codon.

Figure 1-1a: Computer generated model (SWISS MODEL) for KatG heme-containing

Following on the structure in Figure 1-1a and gene analysis, cloning of KatG gene into a bacterial high expression pBAD vector system has been completed successfully. To purify the protein using nickel nitroloacetic acid resin (Ni-NTA), a hexahistidine-tag (6xHis) was introduced at the C-terminal by the cloning primers. Furthermore, in order to introduce unnatural amino acid, DOPA, the TAG codon mutation has been introduced at Y559 position.

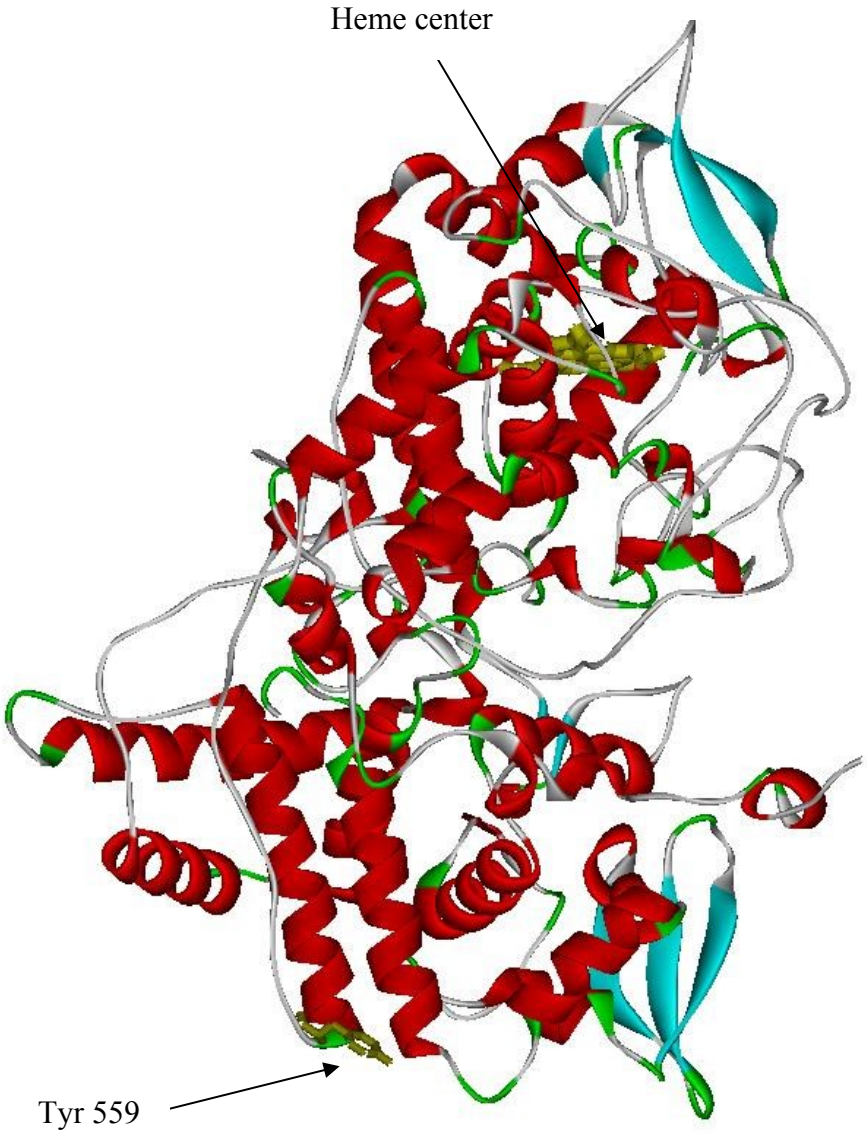

Figure 1-1b: DOPA was incorporated at Y559 position of the KatG

The genetic-incorporation of unnatural amino acid DOPA into proteins was carried out in response to the amber stop triplet codon (UAG) in bacteria.[19-22] This was done using an orthogonal nonsense suppressor PAC plasmid carrying (with tetracycline marker) tRNA/aminoacyl-tRNA synthetase pair derived from the *Methanococcus janannaschi (Mj)* tyrosyl tRNA/aminoacyl-tRNA synthetase pair which is selectively

evolved to recognize the DOPA substrate in *E. coli* expression strains.[23-24] Therefore in this chapter we focus on the genetic incorporation of the DOPA unnatural amino acid by site-directed mutagenesis at the position Y559 in KatG (Figure 1.1b) as well as the expression and purification of the WT KatG enzyme. The incorporation of DOPA takes place during protein translation *in vivo* therefore the natural biosynthesis machinery for protein will ensure the native inside the cell.[25] Using this site-specific incorporation method, fully functional proteins with a unique reactivity acquired with an incorporated DOPA can be employed to carry out (described in chapter 2) to tag KatG onto the surface.[26]

1.2 Materials and Methods

1.2.1 *Chemicals and Media Preparations*

Analytical grade or higher quality of chemicals was used. Luria-Bertani (LB) broth was prepared as follows. Per one liter of LB medium contains 10 g tryptone, 5 g yeast extract and 10 g sodium chloride. LB medium was autoclaved to get it sterilized and added with required antibiotic before the culture growth. Luria-Bertani (LB) Agar plates consisted of 10 g casein peptone, 5 g yeast extract and 10 g sodium chloride were prepared by dissolving in the Milli Q water, followed by autoclaving. Before usage, LB agar was melted in the microwave and poured into Petri dishes after adding the required antibiotics. 2xYT broth was prepared using 2x Yeast extract, 16 g tryptone, 10 g yeast extract, and 5 g NaCl, and the corresponding antibiotics. Primers were designed using Vector NTI program (Invitrogen).

1.2.2 *Preparation Method for Electrocompetent DH10B E. coli Cells*

DH10B cells were purchased from Invitrogen has propagated to make stocks for further use. Initially, the 1 liter culture was incubated at 37 °C until OD_{600} reached to

0.5. Then ice-cold culture was transferred to centrifuge tubes and centrifuged at 5000 rpm for 8 min. at 4 °C in a Beckman centrifuge.

The cells were collected by decanting the supernatant and resuspended in sterilized ice-cold water. Cells were washed three times with cold water containing sterilized 10% glycerol/water (v/v). After decanting residual 10% glycerol/water liquid solution was used to resuspend the electrocompetent cells and stored them as 100 µL aliquots in -80 °C freezer.

1.2.3 *Preparation of DNA Agarose Gel*

5 µL of ethidium bromide was added to 200 µL of Agarose in TAE (1X) buffer solution. DNA 10 µL combined with blue juice (Invitrogen) was loaded into the Agarose gel wells. 1Kb DNA ladder (Promega) was used for DNA size estimation. Gel electrophoresis was carried at 125 V for 45 minutes. The DNA bands were visualized in a UV transilluminator.

1.2.4 *KatG Gene Isolation and Amplification using PCR*

Construction of the plasmid carried out using the gene of WT KatG, was inserted into the *Nco I/Kpn I* sites of the pBAD vector (Novagen, Madison, WI, USA). Catalase-Peroxidase was isolated directly from genomic DNA using 5'-ATAAGACTACCATGGGACTAAAGAAAATTGTAACTGCTTTAGGAATGTCTG-3' (forward) and 5'-CCAGATGGTACCTCAATGGTGATGGTGATGATGCTATTGTTGAACATCAAATCTGCC AAGC -3’ (reverse) primers with a C-terminal 6xHis tag. Site-directed mutagenesis was carried out using a PCR-based Phusion site-directed mutagenesis kit (NEB, Ipswich, MA, USA) and an amber (TAG) mutation was introduced into the wild-type gene sequence in the following position using the forward and reverse primer sequences as indicated in Y559(TAG) KatG; forward 5’-CTAAACAAGCTGGTTAGAATATACAAATGCC-3’, reverse

5’-CTGCTTGCTCAACACCCACATTACC-3’. PCR was carried out in an MJ Mini thermal cycler (Bio-Rad) using the PCR program in Table 1-1. The PCR product was purified using MinElute PCR purification kit (QIAGEN) following manufacturer’s instructions.

Table 1-1 PCR conditions for gene amplification

Component	Amount
5x Phusion HF	5 (1X)
10 mM dNTPs	1 µL (200 µM each)
10 µM Forward primer	1 µL (0.2 µM)
10 µM Reverse primer	1 µL (0.2 µM)
Template DNA	1 µL (250 ng)
Phusion DNA polymerase	0.5 µL (1 unit)
Ultra pure nuclease-free water	to 50 µL final volume

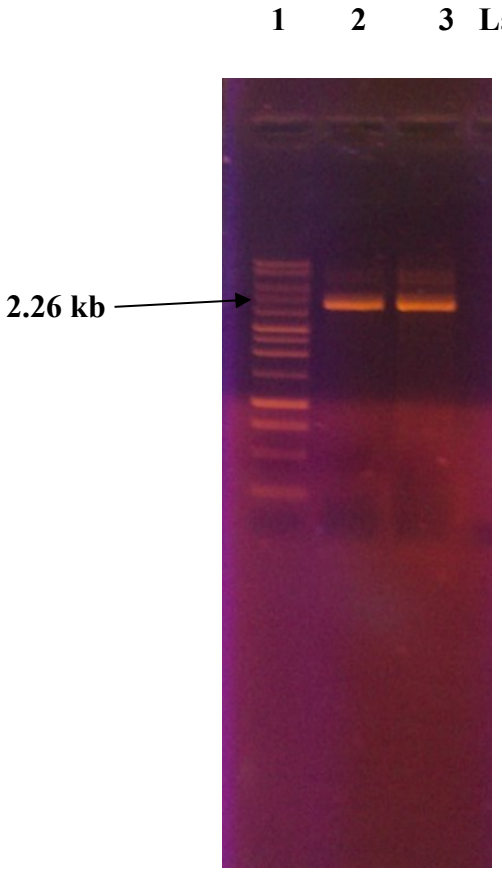

Figure1-2: The DNA agarose gel of KatG analysis. Lane 1: DNA 1 kb ladder; Lane 2: WT KatG; Lane 3: mutant KatG

1.2.5 *Restriction Digestion of KatG Gene and Preparation of pBAD Plasmid Construct*

1.2.5.1 KatG Gene Digestion

The purified PCR product of the KatG gene was digested with NcoI and KpnI restriction enzymes (New England Bio Labs) following the conditions mentioned in Table 1-2 by incubating at 37 °C for 2h. The digested product was purified as mentioned above using the MinElute PCR purification kit (QIAGEN) following manufacturer's instructions. 1% (w/v) agarose gel electrophoresis was used to analyze the DNA extract.

Table 1-2 Restriction digestion chart for KatG

Component	Amount
10X NEB I	5 µL (1X)
BSA	0.5 µL
Template DNA	1 µg
NcoI	1 µL
KpnI	1 µL
Ultra pure nuclease free water	to 50 µL final volume

1.2.5.2 pBAD Plasmid Preparation for Cloning

The plasmid was isolated from a culture (10 mL) grown to OD_{600} 0.5 with QIAprep Spin Miniprep Kit (QIAGEN) according to manufacturer's procedure. The pBAD plasmid was digested with NcoI and KpnI restriction enzymes (New England Bio Labs) to obtain the sticky ends for The KatG gene cloning with incubation at 37 °C for 2h. Digested pBAD vector was isolated from gel electrophoresis in a 0.6% agarose gel. The correct band of the gel was separated using a blade and the digested DNA plasmid was extracted using MinElute Gel Extraction Kit (QIAGEN).

1.2.6 *Recombinant Plasmid*

Recombinant Plasmid was prepared by ligating the NcoI and KpnI digested and purified KatG gene with digested (similar way) pBAD plasmid. T4 DNA ligase was used in a 1:3 ratio of plasmids with insert in 10x ligase buffer. After incubating for 1h at room temperature, the 1 µL of the purified (using PCR purification kit) was transformed into *E. Coli* DH10B cells.

1.2.7 *Transformation of the Recombinant Plasmid into DH10B Cells*

Electrocompetent *E. coli* DH10B cells were transformed with the recombinant plasmid (both WT gene as wells as the mutant KatG) by adding 3 µL to a 50 µL aliquot cells. The mixture was transferred to a pre-chilled MicroPulser electroporation cuvette for electroporation in a MicroPulser electroporator (Bio-Rad). The cells were recovered with 300 µL of freshly prepared sterilized S.O.C. medium and incubate 1h at 37 °C. Transformed cells were streaked onto a LB agar plate with ampicillin. After overnight incubation at 37 °C, selected bacterial colonies were hand-picked after grown in 5 mL LB culture tubes for DNA sequencing after miniprep purification. Gene sequences were analyzed using Vector-NTI program (Invitrogen) and confirmed its accuracy.

1.2.8 *Expression and Purification of WT KatG and Its Mutant*

1.2.8.1 Purification of WT KatG

Recombinant plasmid of pBAD N-term 6xHis tag added KatG was transformed to DH10B *E. Coli.* The expression host was grown at 37 ^{0}C in LB medium containing 100 µM of ampicillin until OD_{600} value reached ~0.8. 0.2% arabinose was then added to induce the KatG expression for 8 hours at 30 ^{0}C. Cells were harvested by centrifugation (10,000 rpm) and lysed in lysis buffer (50 mM Tris, 100 mM NaCl at pH 8.0). The protein is purified under native conditions. The cell suspension was treated with 80 µL Lysozyme (100 mg/mL), 40 µL DNase I (5 mg/mL) and 40 µL of RNase A (100 mg/mL). The cell suspension was stirred at 4 ^{0}C for 1h to allow lysis to occur. The clear supernatant after centrifugation at 9,000 rpm, 4 ^{0}C was loaded onto a nickle nitroloacetic acid resin (Ni-NTA) (Qiagen,Hilden,Germany) and eluted to afford ~10 mg/L of protein.

1.2.8.2 Purification of Y559(DOPA) Mutant KatG

In our lab we incorporate UAA (DOPA) at specifically designed site in proteins by introducing an amber (TAG) mutation into the wild-type gene sequence. The cotransformed cells with (Y559TAG) KatG containing pBAD plasmid (Amp marker) and PAC(DOPA)RS-6tRNA (Tet marker) were grown in glycerol minimal media (GMML) supplemented with ampicillin and tetracycline. The culture was incubated at 37 °C with shaking until OD_{600} reached 0.5. Then DOPA (1 mM) was added to the 1L culture followed by induction with 0.2% arabinose. Culture temperature was reduced to 30 °C, and the culture was kept in the shaker for overnight. The cells were lysed in lysis buffer (50 mM Tris and 100 mM NaCl, pH 8.0) with 80 µL of Lysozyme (100 mg/mL), 40 µL of DNase I (5 mg/mL), and 40 µL of RNase A (100 mg/mL) under stirring with a stir bar for 30 min at room temperature followed by three freeze (liq. N_2) - thaw (37 °C) cycles. Sonication on ice for 1 min on and 1 min off intervals (for 3 consecutive times), the cell debris was removed by centrifugation at 5,000 rpm for 30 min before the His-tagged protein was purified using nickel nitrilo-triacetic acid Ni-NTA resin (QIAGEN). The resin-bound protein was subjected to a column, and protein was eluted with imidazole containing buffer (300 mM NaCl, 250 mM imidazole, 50 mM phosphate buffer, pH 8.0). Analysis was done using sodium dodecyl sulfate-polyacrylamide gel electrophoresis (SDS-PAGE) in a precast gel (Novex Tris-Glycine). Dialysis was used to remove the excess imidazole before storing at -80 °C in potassium phosphate buffer (100 mM, pH 7.4) until further use.

1.3 Results and Discussion

As shown in Figure 1-3, 1-4 and 1-5, I have carried out successful isolation of KatG gene from genomic DNA from *Francisella tularensis*. Isolated gene was cloned into

a pBAD (with Ampicillin resistant marker) plasmid. This C-terminal 6xHis tag KatG gene was transformed into *E. Coli* DH10B cells and grown under specific conditions to produce KatG WT and mutant proteins.

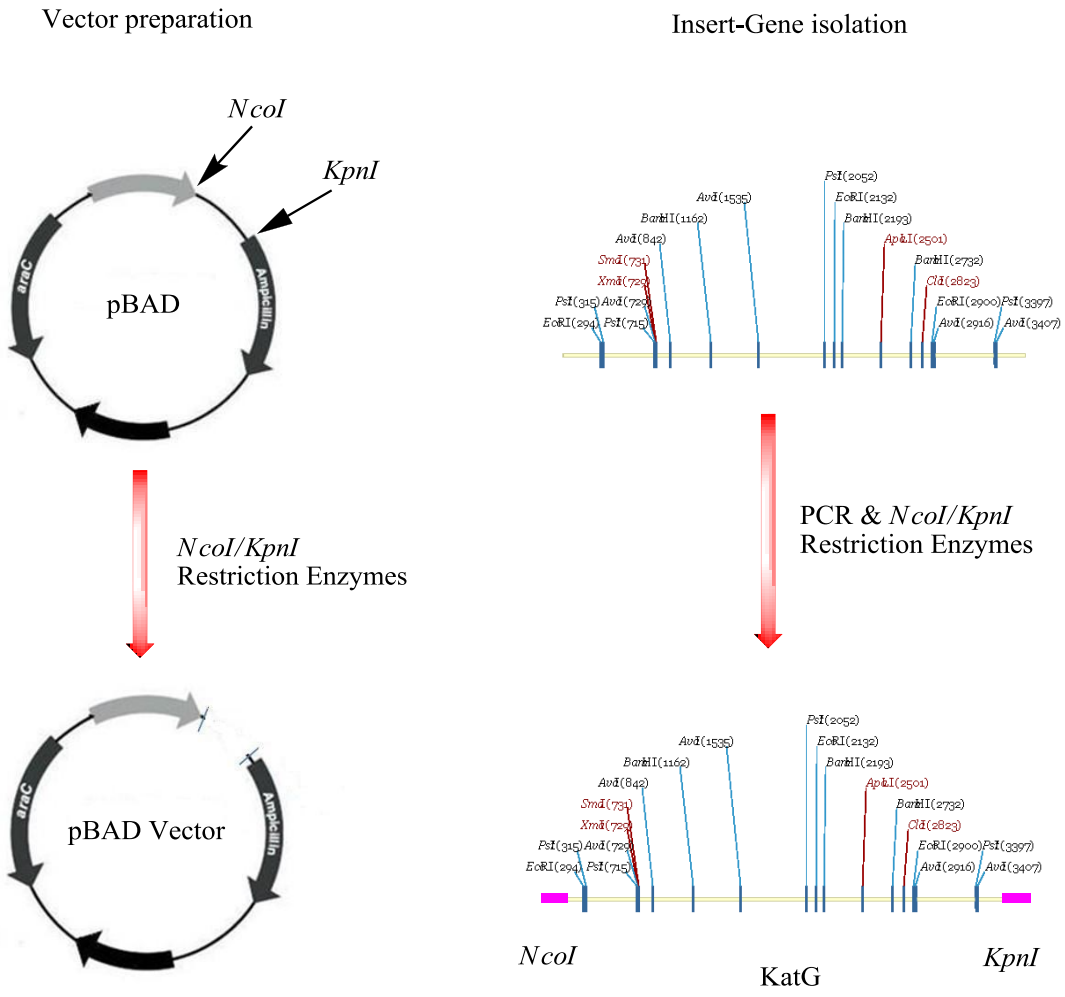

Figure 1-3: Schematic representation of pBAD plasmid and KatG gene isolation.

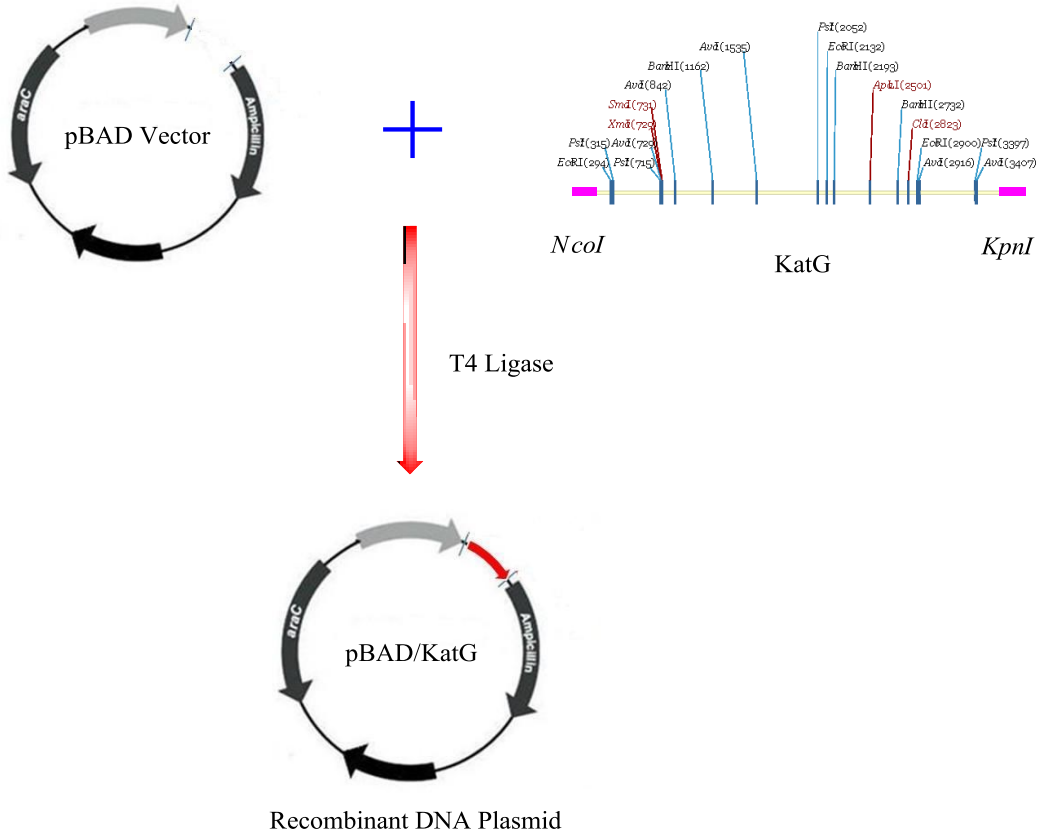

Figure 1-4: Schematic representation of ligation of pBAD plasmid and KatG gene.

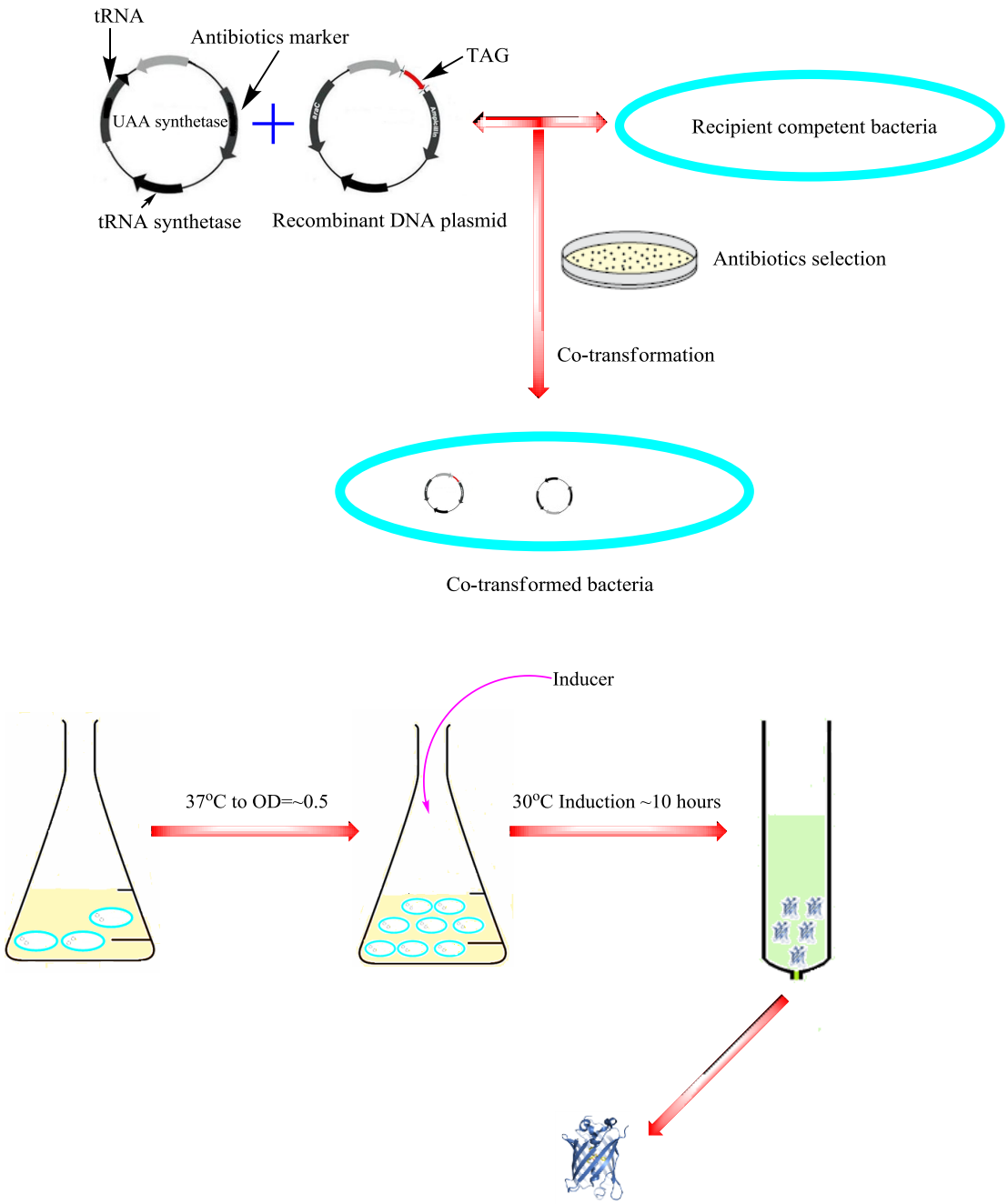

Figure 1-5: Schematic representation of recombinant DNA plasmid transformation into *E. Coli* DH10B cells for protein expression.

E. coli expression has been carried out using LB medium at 30 °C for WT and mutant KatG as described in the method section. Ni-NTA purification using specially our own protocol ensured the highest purity of the protein. Analysis by SDS-PAGE confirmed the protein to be >95% pure. Furthermore, it had also showed the monomer around 82.5 kDa and a small amount of dimer around 165 kDa, as expected for this protein. (Figure 1-6)

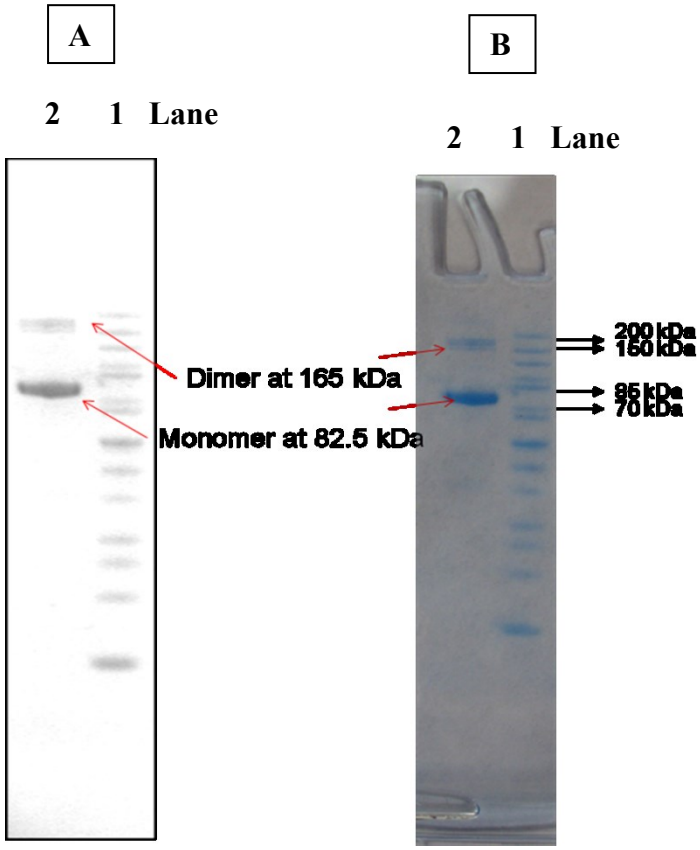

Figure 1-6: Coomassie-stained SDS-PAGE analysis of (**A**) WT KatG and (**B**) mutant KatG with DOPA. Lane 1, molecular weight standards as indicated in kiloDalton (kDa), and Lane 2, expressed protein.

DOPA was incorporated at TAG Amber codon at Y559 of KatG gene. TAG was generated in the gene via site-directed mutagenesis using primers containing the

mutation. Sequence analysis confirmed a successful mutation. As discussed in method section, Y559(DOPA) mutant KatG was co-expressed with the PAC-DOPA RS-6tRNA synthetase plasmid encoding for $tRNA_{CUA}$/aminoacyl-tRNA synthetase pair in order to incorporate the DOPA unnatural amino acid during protein translation.

Finally, the WT and mutant KatG with C-terminal 6xHis tag tail for Ni-NTA protein purification were successfully cloned into pBAD plasmid. Expressed proteins using our new protocol were found to be quite pure, above 95% and were used for protein tagging onto a surface as described in Chapter 2.

Figure 1-7 shows the electronic absorption spectra of WT KatG (blue line) and Y 559(DOPA) KatG (red line). The overlays of spectra suggest that there is no protein conformational change during the mutant translation and followed protein folding.

The Soret absorption for wild-type falls in the 406 nm ($\lambda_{max} = 406$) region, while the Y559(DOPA) KatG is 1 nm red-shifted to higher wavelength with $\lambda_{max} = 407$. This is may be due to the influence by the DOPA incorporation at Y559 position of the KatG on the protein conformation.

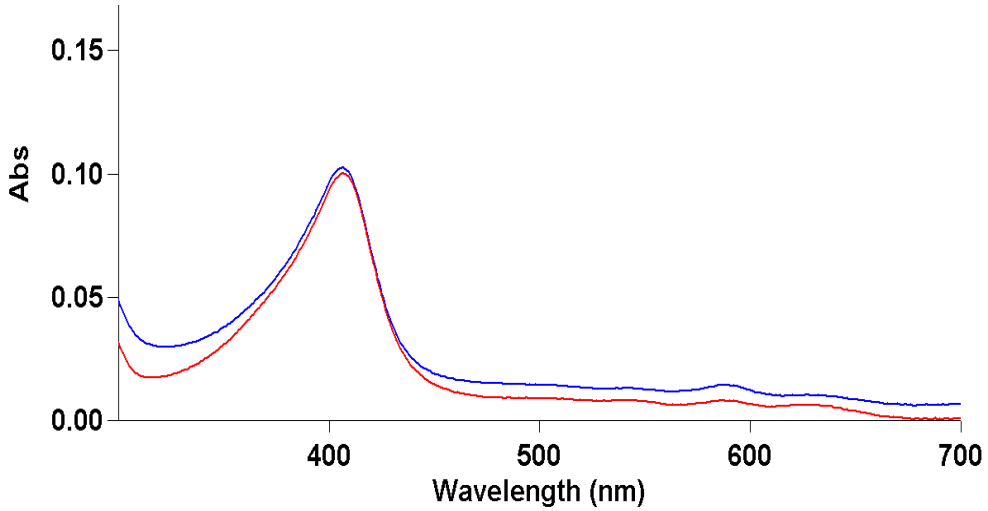

Figure 1-7: Electronic Absorption spectra of WT KatG (blue line) with λ_{max} = 406 nm and Y559(DOPA) KatG (red line) with λ_{max} = 407.

1.4 Conclusion

Successful Y559(TAG) codon insertion into the KatG gene was confirmed by DNA sequencing. Based on Electronic Absorption spectra (the Soret at 405 nm) has confirmed the native folding of both WT KatG as well as Y559(DOPA) mutant KatG enzymes. This suggests our mild purification technique had produced the native and active protein during protein expression. Genetic incorporation of DOPA into KatG protein can be used to accomplish the follow up site-directed surface tagging. Next chapter we will discuss the surface covalent attachment and its activity confirmation using peroxidase function of KatG via the H_2O_2 mediated 2-naphthol polymerization reaction.

Chapter 2

Introduction of Novel Michael Addition Reaction for the Surface Immobilization of Enzymatically Active Protein Y559(DOPA) Mutant KatG

All the experiments in this chapter were done by Yanbo Zhang in the laboratory of Prof. Roshan Perera.

2.1 Introduction

Molecular oxygen is capable of producing potentially living cell toxic reactive oxygen species such as superoxide, hydroxyl radicals and H_2O_2.[2,27-28] The KatG from *F. tularensis* can decompose the H_2O_2 when presence in lethal level. KatG is a bifunctional heme-dependent enzyme with catalase and peroxidase activities embedded to it.[2,18,29] Catalase is present in virtually all aerobic organisms and many anaerobic organisms including humans and is well known to decompose H_2O_2 to dioxygen and water.[28] Though these enzymes have extensive structural similarity, studies have shown the many of their properties are different. There are salient variations of 10 to 1000 times in specific activities, reaction velocities, sensitivity to damage by the substrate H_2O_2, and sensitivity to inactivation by inhibitors and heat.[13] Unlike KatG, naturally occurring catalases need reduced NADPH cofactor to prevent accumulation of inactive compound II (Figure 2-1).[13] Therefore, an extensive supply of NADPH is required to decompose H_2O_2 by preventing inactivation. Due to the fact that catalase activity depends on reduced form of NADPH cofactor, their practical usage of catalase is limited.[30]

On the other hand KatG does not require a reduced NADPH or NADH to carryout activation of compound II. This is because peroxidase nature of heme (with proximal histidine) would not allow the accumulation of compound II in the presence of H_2O_2.[31]

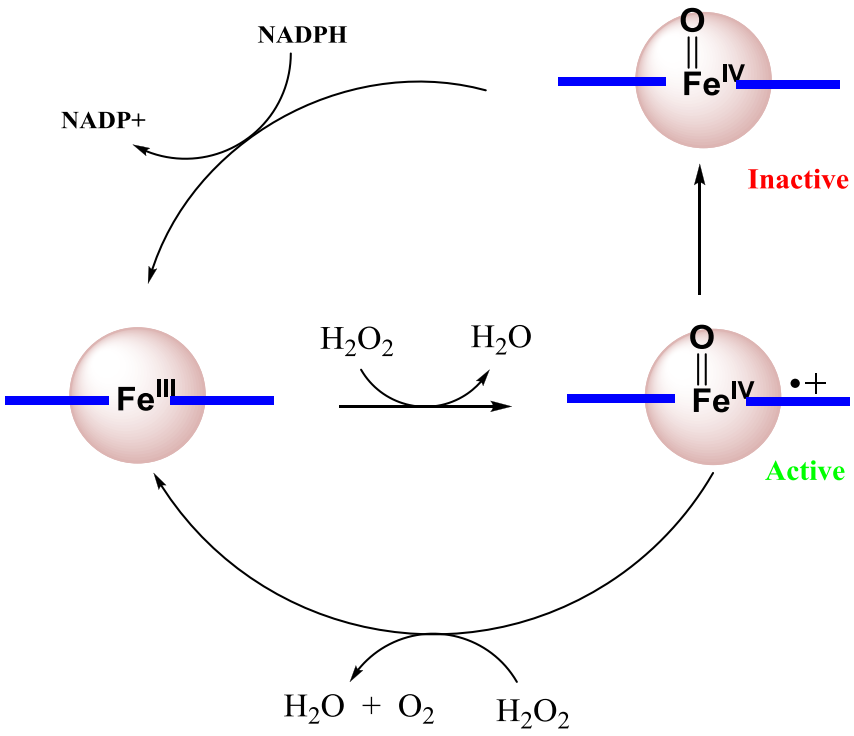

Figure 2-1: The catalase catalytic reaction. KatG is also presumed to function similar way.

In 2005, *F. tularensis* genome was sequenced completely. Hence, the overexpression and characterization of this enzyme allows us now to report its catalytic properties and an investigation of the mechanism of the enzyme's reaction kinetics. Herein, we use the reaction of naphthol polymerization of the surface-bound KatG to show its peroxidase activity.[32-33] Furthermore, this reaction was carried out with silica chip-bound KatG (bound to silica or magnetic nanoparticles, polypropylene, PMMA etc.) which provides the versatility of usage of this protein in industry applications.

Polymerization reaction of 2-naphthol generates a hydroxylated polynuclear aromatic hydrocarbon that is widely used in the production of dyes, plastics,

pharmaceuticals, synthetic fibers, rubbers, and pesticides.[34-35] 2-Naphthol in the soil and water has a significant impact in the environment since 2-naphthol is a potential carcinogen.[36] Furthermore, during accidental spills or leaks or through discharge of industrial waste waters naphthol can be introduced to environment as a pollutant. Polymerization of 2-naphthol using peroxidases has been used to eliminate the phenolic naphthol from water.[35,37] Hence enzyme-mediated oxidative polymerization of naphthol into naphthol polymerization products (as insoluble oligomers) will be a useful technique to precipitate out naphthol from a solution.[35]

Previous studies with laccase-catalyzed oxidation of 1-naphthol generated average molecular weight of naphthol polymerization products (NPPs) around 4.92 kDa which is insoluble violet precipitate. Horseradish peroxidase (HRP)-mediated oxidation of 1-naphthol at pH 7 showed increase turnover numbers for NPPs.[35,37] Researchers have proposed HRP-mediated oxidation as a treatment method for water contaminated with naphthol. However, the impact of solution chemistry on naphthol transformation remains largely unknown. The goal of this chapter is to facilitate the elimination of 2-naphthol from contaminated water using a continuous flow bioreactor with immobilized KatG protein, the enzyme based approach to treat waters contaminated with hydroxylated polynuclear aromatic hydrocarbons such as naphthol.

2.2 Materials and Methods

2.2.1 *Chemicals.*

DOPA, $NaIO_4$, 2-naphthol, NaOH were purchased from Sigma-Alrich. H_2O_2 (30% w/w, 8.82 M) was purchased from Aldrich Chemicals Co., stored at 4 °C, and used without further purification.

2.2.2 *WT KatG Expression and Purification*

C-terminal 6xHis tag added Y559(DOPA) mutant KatG gene from species *Francisella tularensis Schu 4* in *E. Coli* expression host was expressed as explained in Chapter 1.

2.2.3 *Functionalization of the Surface*

Functionalization of silica surface is important for proper immobilization of active proteins on a solid amine surface via a Michael addition bioconjugation reaction in water. Furthermore, silica surface gives homogenous platform to the reaction mixture. Therefore, starting with a free amine surface, further functionalization of the support system can be done with the serial application of two reactions: activation and extension.[38] To obtain the initial surface, amine-coated silica nanoparticles (NPs) will be synthesized by a one-pot reaction. Homogenous silica NPs will be synthesized based on the sol-gel method developed previously.[38-39] The synthesis consists of the hydrolysis of tetraethoxysilane (TEOS) and its subsequent condensation in a water/ethanol solution with ammonia as a morphological catalyst. By adjusting the reaction parameters, such as water and ammonia concentration, the particle size and monodispersity will be controlled.

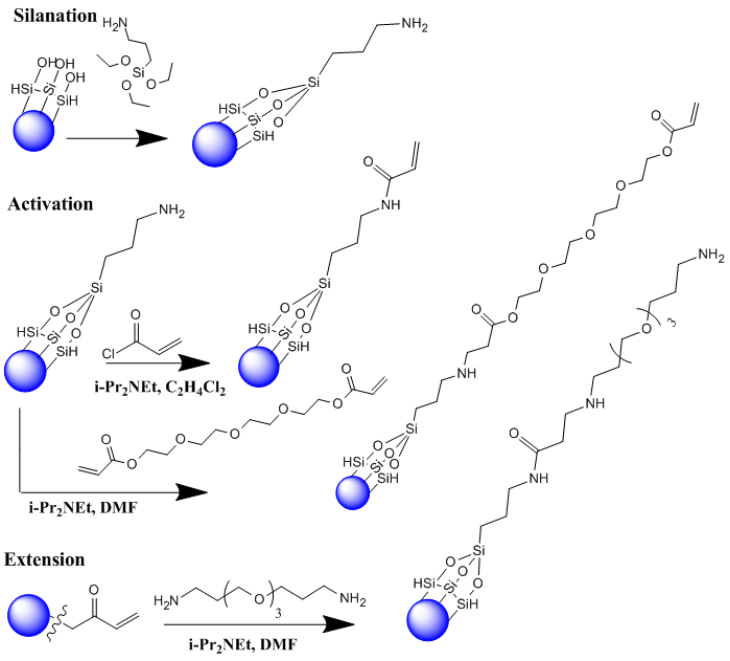

Figure 2-2: Reaction steps for functionalization of silica surface.

The uniformly distributed silica was silanised with 3-aminopropyltriethoxysilane (APTES) in the same reaction mixture by a simple reflux. Alternatively, the initial surface can be obtained by mixing TEOS and APTES together during the synthesis, thus giving an “organo-silica sphere”. Although each method ultimately gives the same product, some properties such as mass density, microporosity, and siloxane structure may differ. Furthermore, NPs coated with APTES on the surface can be grown larger by adding another silica layer from TEOS. By having a variety of properties to choose from, the method best suited for immobilizing proteins can be determined. The amine surface can be activated by either acylating the amine with acryloyl chloride or adding the amine to the unsaturated β position of the acryloyl group from tetraethylene glycol diacrylate, both giving an acryloyl terminated surface as shown in Figure 2-2. The surface will be

extended by the addition of an amine linker to the unsaturated β position of the surface acryloyl group, thus increasing the distance between the functional group and the support. The terminal free amine can then be activated as before. The surface of the support will be able to provide an environment conducive to protein stability by choosing a polyethylene glycol (PEG) like linker such as 4,7,10-Trioxa-1,13-tridecanediamine and tetraethylene glycol diacrylate.[40] PEG provides a lipid or glycerol like environment that proteins are naturally surrounded in and allows silica NPs to be more miscible with the water solvent. Furthermore, the highly flexible groups will not introduce any unnecessary steric hindrance during protein tagging. This two-step process can be repeated until the desired length is obtained. The reactions will be monitored by the Kaiser Test, i.e., staining the silica gel after each reaction with ninhydrin. Free (primary) amines will give a deep purple colour, known as Ruhemann's purple, and secondary amines will be yellow-orange in color. The presence of the acryloyl functional group will be monitored by infrared spectroscopy (IR).

2.2.4 *Surface Attachment of Y559(DOPA) Mutant KatG*

DOPA quinone mediated bioconjugation reaction was carried out in WT KatG containing Kphos buffer at pH 6.0 with $NaIO_4$ for 2h gentle shaking at room temperature. Fresh WT and mutant KatG were used for immobilization within 2h after preparation. The method involves (to control the protein orientation and also carry out a formation of a strong permanent linkage with the solid support-containing amine group) the addition of a mild oxidant (~100 μM sodium per-iodate $NaIO_4$) to Y559(DOPA) mutant KatG at room temperature for 2h. Addition of sodium per-iodate ($NaIO_4$) to the Y559(DOPA) KatG will give a highly reactive DOPA-quinone. This native modified protein can be then used for

Michael addition reaction with silica surface.[41] Amine groups on silica surface react with DOPA-quinone to form a strong covalent bond and can be used to attach proteins.

2.2.5 *Atomic Force Microscope (AFM) Imaging*

Veeco MultiMode V SPM performed the surface topography of mutant KatG tagged amine-functionalized glass slide.

2.2.6 *Potassium Permanganate Titration with H_2O_2*

Catalase activity of KatG was measured as follows: 1 mL of 3% H_2O_2 solution with WT and mutant KatG tagged glass beads was taken to titrate with 10 mM potassium permanganate at different time intervals.

$$5\ H_2O_2(aq) + 2\ MnO_4^-(aq) + 6\ H^+(aq) \rightarrow 2\ Mn^{2+}(aq) + 5\ O_2(g) + 8\ H_2O(l)$$

2.2.7 *2-Naphthol Polymerization*

To a solution of 1 μM mutant KatG in 20 mM buffer, 1 mM of 2-naphthol was added, 25 mM of H_2O_2 in water was added to initiate the polymerization reaction.[37] Working solutions of H_2O_2 were prepared by diluting 30% w/w H_2O_2 with distilled/deionized water and were used within 1h of preparation. Preliminary experiments showed that addition of only KatG or only H_2O_2 at the concentrations used in this study resulted in no significant transformation of 2-naphthol. KatG was dissolved in distilled water to make solutions of approximately 2 μM and used within 0.5h of preparation. High purity 2-naphthol (>99%) was purchased from Sigma Chemicals and a stock solution (1.1 M) was prepared by dissolving 2-naphthol in methanol. The stock solution was stored at 4 °C and working solutions were prepared by diluting stock solutions in various pH buffers.

2.3 Results and Discussion

2.3.1 *Immobilization of the Native and Functional Protein on the Surface*

Current methods for the direct attachment of protein molecules to solid supports results in a random orientation of the protein and deformation of structure due to harsh chemical tagging conditions.[42-43] Traditional methods for protein immobilization onto solid supports have been based on physical adsorption, noncovalent binding to surfaces, entrapment in semi-permeable membranes, and microencapsulation/sol-gel methods into polymer microspheres and hydro-gels.[44-47] The most popular method for protein immobilization onto solid supports is through noncovalent interactions, obtained by the use of streptavidin/biotin or recombinant affinity-tagged proteins.[48-50] However, the binding interactions may not be stable, resulting in escape of the protein from the solid surfaces. Hence we will be developing novel immobilization methods to address these concerns based on three mild reactions. The immobilization of KatG was designed using genetically encoded DOPA amino acid. The data suggest that the immobilization method produces relatively homogeneous and active protein on the surface.

Furthermore, our lab has the ability to incorporate new additional amino acids at defined sites with different chemical groups inside living organisms (i.e., bacteria). The genetic incorporation of DOPA with an amber codon (TAG) will generate novel features for proteins while retaining native conformation, like forming a strong permanent linkage between DOPA and amine derivatized solid through Michael addition reaction (as in Figure 2-2).

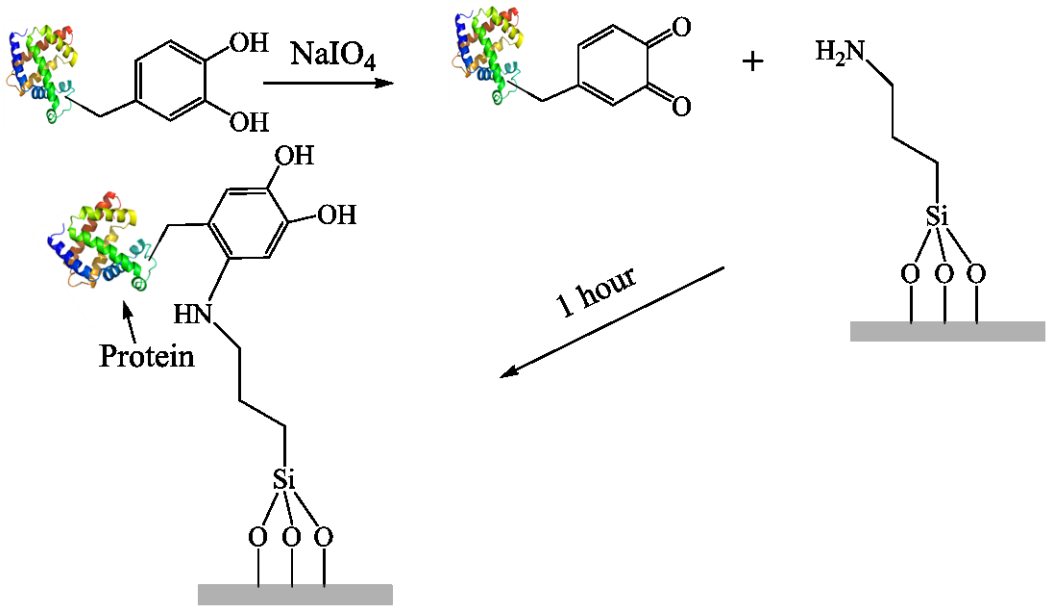

Figure 2-3: Schematic representation of Michael addition reaction in DOPA-containing protein

Besides the method introduced above to incorporate UAA into proteins, another method used in our lab is the Selective Pressure Incorporation (SPI) which can allow us to replace all the tyrosine residues with DOPA. The purpose is to enhance the immobilization efficiency with more protein being tagged to the solid surfaces. Michael addition reaction can then be employed to bioconjugate the mutant protein onto derivatized solid surfaces.

In this chapter, I will describe the incorporation of additional functional groups, such as quinones, (a) to create covalent linkages via the Michael addition reaction, (b) expression and purification of the native wild-type KatG and mutant KatG in solution before tagging on to the surface, (c) site-directed attachment of the DOPA containing

mutant proteins onto a solid support, (d) generation of a protein that retains its native conformation and thus fully active and functional, (e) monitoring the color change kinetics of the 2-naphthol polymerization using UV-Vis spectroscopy and monitoring the product using mass spectroscopy.

As describe in Chapter 1, in the absence of conformational change for the genetic incorporation of neurotransmitter/hormonal precursor 3, 4-dihydroxy-L-phenylalanine Y559(DOPA) KatG protein and now we will look into the functional properties of this mutant. This novel approach holds a great promise for wide spread applications and it opens a new door in biotechnology application from drug-discovery to industrial bioreactors.

Furthermore, protein bioconjugation or attachment to a surface plays an important role in the development of effective vaccines, affinity column chromatography techniques, drug-delivery systems and functional protein microarrays. Generally, protein–surface conjugation methods rely on chemoselective modification of natural amino acids of protein. In general, these reactions are harsh and end up with denatured proteins. Naturally occurring residue of chemical modifications can lead to the loss of protein activity and its functional properties. Therefore, surface tagging is a major challenge in arrays preparation.

In order to address these challenges, we have developed separate protocols for the functionalization of the surfaces (total of seven protocols have been developed), such as polypropylene surface, borosilicate glass surface, pyrex glass surface, silica gel surface, polystyrene surface, poly(methyl methacrylate) [PMMA] surface and gold or metallic surface for protein tagging. The functionalized surfaces were characterized using methods, such as Atomic Force Microscopy (AFM), X-ray photoelectron spectroscopy (XPS), electrochemistry etc. Furthermore, each derivatization protocol has been

optimized to get the optimal tagging based on KatG attachment method. In addition, optimal tagging was confirmed and quantified by following the activity of the surface-bound proteins. These different surfaces will bring the versatility (make it easy for the development of marketable product) and novel phenomena to the protein immobilization work proposed in this project.

For the DOPA containing KatG mutants (Amber condon method), Michael addition was carried in water or buffer between oxidized DOPA (quinone) and amine-derivatized solid surface, with mild oxidant sodium per-iodate. $NaIO_4$ mediates the direct binding between Y559 (DOPA) mutant KatG and the primary amine-derivatized porous glass beads, with the presence of oxidized DOPA quinone moeity on the protein surface. Thus, the successful generation of a functional protein array paves the way for novel bioreactor development.

Immobilization work is based on creation of a covalent bond through a simple mild reaction (in the absence of any harsh chemicals, such as chelating ligands, catalysts and organic solvents) in a very short time. The reaction was carried out at room temperature, to generate a homogenous protein layer following the reaction described in method section and confirmed by the AFM data (Figure 2-3).

(A)

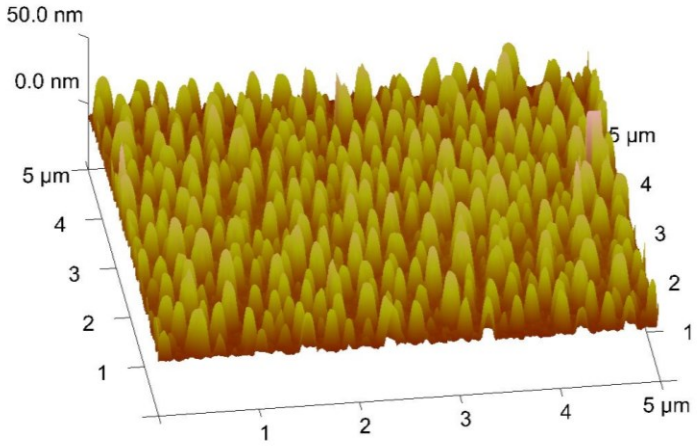
50.0 nm
0.0 nm
5 µm
4
3
2
1
1
2
3
4
5 µm

(B)

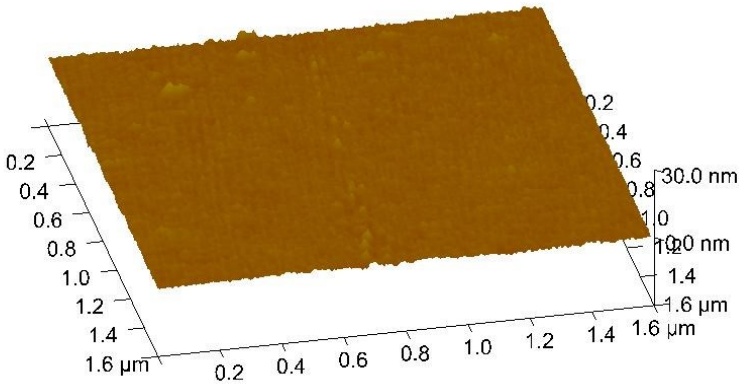
0.2
0.4
0.6
0.8
1.0
1.2
1.4
1.6 µm
30.0 nm
1.4
1.6 µm

(C)

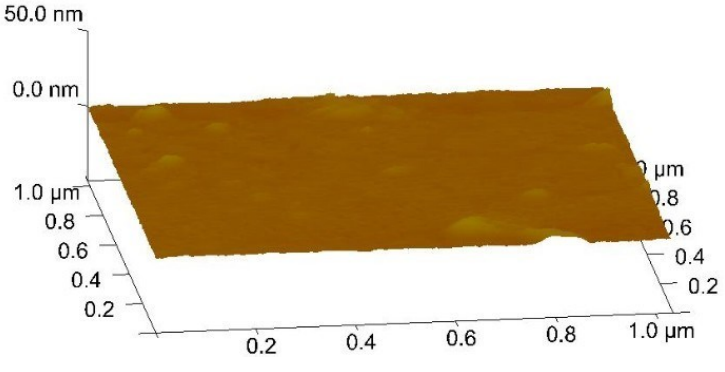
50.0 nm
0.0 nm
1.0 µm
0.8
0.6
0.4
0.2
0.2
0.4
0.6
0.8
1.0 µm

Figure 2-4: (A) AFM topographic image of glass solid support attachment of Y559 (DOPA) KatG mutant; (B) The derivatized glass surface with WT KatG after treatment with 100 μM $NaIO_4$ (control); and (C) Blank but amine functionalized glass chip. Both (A) and (B) were taken after the reaction with protein in the presence of 100 mM of $NaIO_4$. The reaction was carried out in the 100 mM Kphos buffer at pH 7.0.

AFM images were used to visualize the protein arrays on the derivatized glass surface. Unlike the exquisite monolayer created through multi-site covalent KatG mutant attachment with the average height of around 25 nm (Figure 2-4(a)), the $NaIO_4$ mediated covalent binding can achieve drastic increase in the amount of protein tagging on amine-derivatized glass surface due to the random bioconjugation.

As shown in the Figure 2-4, the surface topography of the covalently-attached KatG assemblies were probed by AFM. Figure 2-4 compares the AFM images for a chemically-modified amine-functionalized glass surface before and after covalent attachment of mutant KatG. While the glass surface before protein attachment was featureless (Figure 2-4c), an average feature height of 10-15 nm was observed in the case of the the mutant protein monolayer, which correlated to the actual size of the protein based on the structure generated by us (Chapter 1). On the other hand, covalently-attached WT KatG was unsuccessful as a control experiment, using the same reaction conditions (Figure 2-4c). However, as expected by the absence of the *o*-imino-quinone moiety, the WT KatG did not form a good monolayer on the modified surface. The genetically modified Y559 (DOPA) KatG mutant was succesfully covalently attached onto the amince surface using the Michael addition reaction DOPA quinone moiety of the protein and the amine group on the glass surface. Hence, it can be concluded that the WT KatG did not covalently immbolize on the glass surface in the presence or absence of $NaIO_4$.

Further characterization was carried out using electrochemical methods as shown below. The following results show:

(a) Protein is immobilized in a native confirmation

(b) Protein behaves naturally during catalysis (based on the electron transfer and reversible redox properties)

(c) Data can be used to calculate the amount of protein immobilized on the surface.

2.3.2 *Electrochemistry of Y559(DOPA) KatG Mutant Enzyme*

The electrochemistry of immobilized Y559(DOPA) KatG mutant enzyme on the Au electrodes was studied by cyclic voltammetry (Figure 2-5).

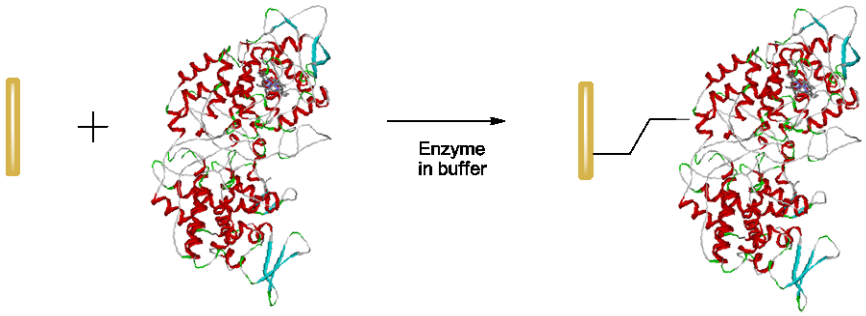

Figure 2-5. Schematic representation of enzyme immobilization on the modified gold electrode surface.

The enzyme was covalently immobilized on the amine functionalized gold surface directly through a mild Micheal addition reaction and it exhibited quasi-reversible redox electrochemistry when examined by cyclic voltammetry from scan rates 10-50 mVs^{-1} (Figure 2-6).

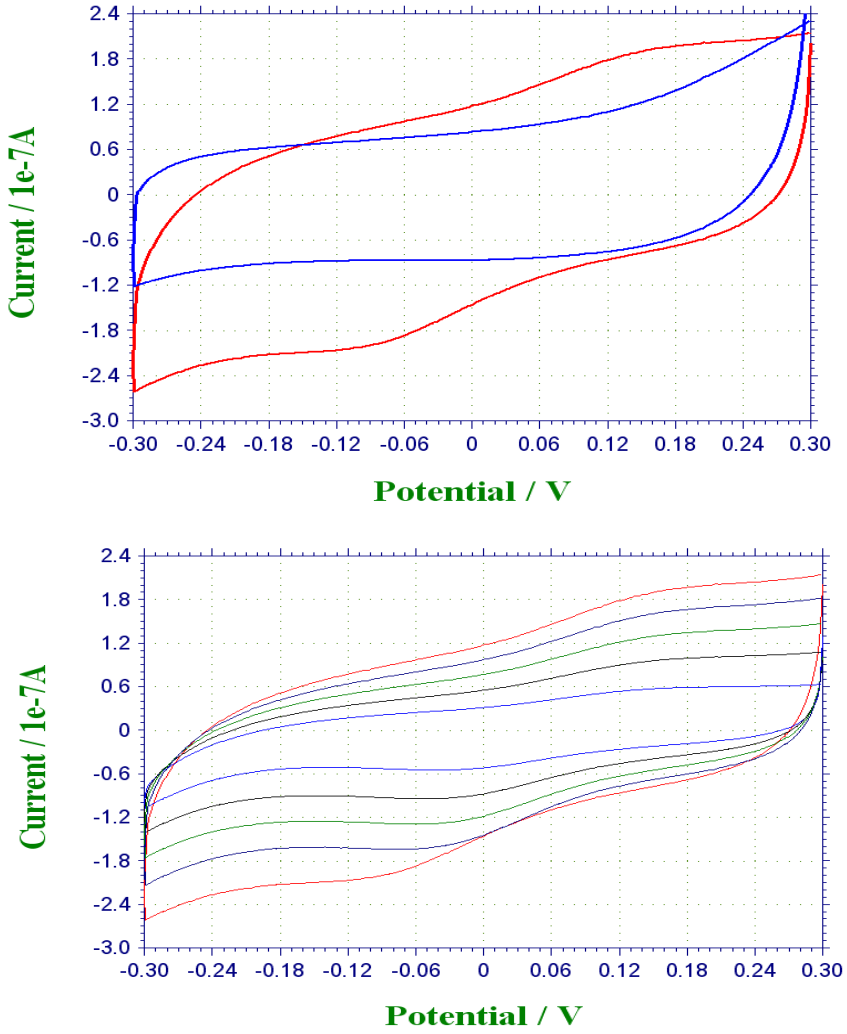

Figure 2-6. (**Top**) Cyclic voltammetry (CV) response of derivatized (blue) and Y559(DOPA) KatG mutant enzyme-immobilized (red) gold electrode in nitrogen-saturated 100 mM phosphate buffer solution (pH 7.0) at room temperature conditions at scan rate = 30 mVs^{-1}. (**Bottom**) CV response of Y559 (DOPA) KatG mutant enzyme-immobilized gold electrode in nitrogen-saturated 100 mM phosphate buffer solution (pH 7.0) at room temperature conditions. Scan rate range = 10-50 mVs^{-1}.

The peak currents were observed to be directly proportional to the scan rates, which show that the proteins were immobilized to the electrode surface. The peak current, I_p for a surface confined reactant is given by:

$$I_p = \frac{n^2F^2}{4RT} A\Gamma\nu \qquad (1)$$

where, n = number of electron transferred, F = Faraday constant, R = universal gas constant, T = absolute temperature in Kelvin (T = 295 K), A = surface area of the electrode, Γ = surface coverage or the concentration of the redox active immobilized in mol/cm^2, υ = scan rate.[51] From equation 1, the slopes of the plots (Figure 2-7) were given by (n^2F^2/4RT)AΓ and substituting the known values, such as the geometric area of the electrode surface (A = 0.0314 cm^2) and the other constants, the estimated values of the number of molecules of the Y559(DOPA) KatG mutant enzyme associated with the electrode surface (Γ) were 4.24 x 10^{-11} mol cm^{-2} for the enzyme immobilized on the modified gold electrode through the mild reaction.

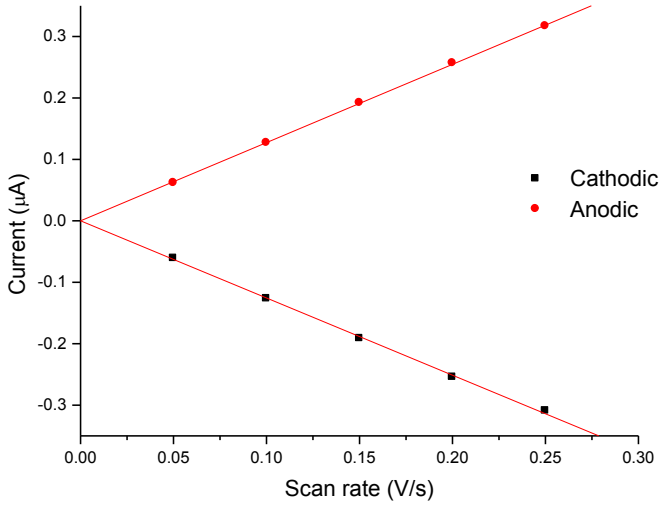

Figure 2-7: Plot of peak current vs scan rate for enzyme immobilized on derivatized gold electrode in nitrogen-saturated 100 mM phosphate buffer solution (pH 7.0) at room temperature conditions. Scan rate range = 10-50 mVs^{-1}.

Since the electrochemical reaction was quasi-reversible in nature, the formal reduction potential $E^{\circ\prime}$ was estimated from the midpoint potential $E_{1/2}$.[51] For the enzyme immobilized on the modified Au electrode, the $E_{1/2}$ was observed to be 58 mV with respect to Ag/AgCl (3.5 *M* KCl) reference.[52-53] The rather large separation of the cathodic and anodic peaks indicated that DET to the protein was slow, but the reversible nature of the reaction proves the enzyme to be catalytically active on the modified surface.

2.3.3 *2-Naphthol Polymerization Product*

Most polymerization experiments were conducted with a 0.5 mM 2-naphthol solution prepared in 20 mM ionic strength at pH 7 in Kphos buffer. Sufficient stock of H_2O_2 was added to solutions to produce an aqueous H_2O_2 concentration of 0.5 mM. Triplicate sets of 13 mL-glass centrifuge tubes were completely filled with the 0.5 mM 2-naphthol solution, and mutant KatG and H_2O_2 were added to initiate the reaction (Figure 2-8). The tubes were immediately capped with Teflon-lined phenolic caps, mixed completely on a touch mixer, and placed on an end-over-end tumbler at room temperature (25 °C). Preliminary experiments revealed that a 3h reaction time was sufficient to achieve complete transformation of naphthol. The contents of the tubes were allowed to react for 3h after which the tubes were removed from the tumbler and catalase added to scavenge any residual H_2O_2 in solution.

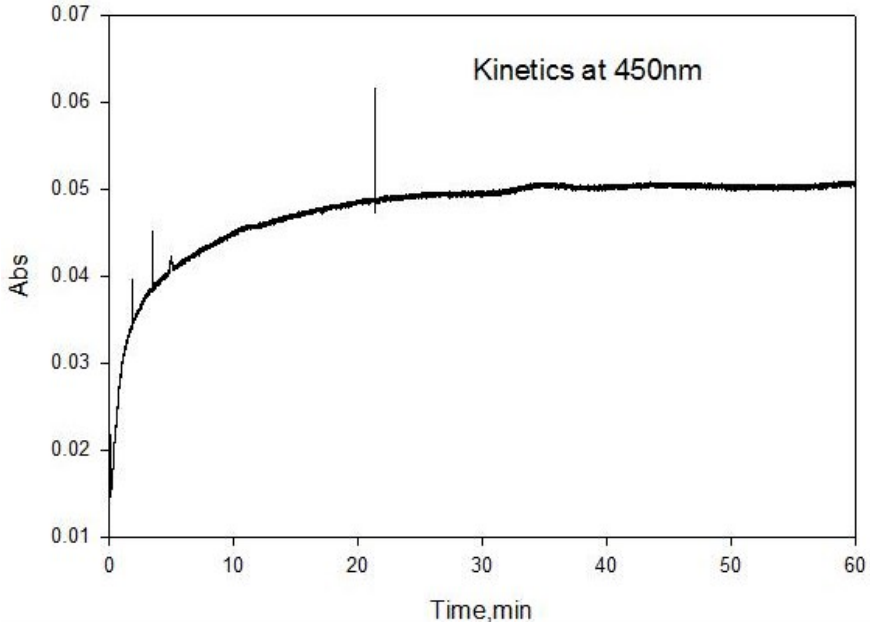

Figure 2-8: Polymerization kinetics of 2-naphthol monitored at λ_{max} 450 nm for silica chip. The reaction mixture had 25 mM H_2O_2, 1 mM 2-naphthol, and KatG-bound chip.

Bifunctional KatG has the ability not only to catalyze the catalase reaction, but also can catalyze the formation of a variety of highly reactive intermediates.[35-36] For example free radicals, according to the enzymatic reaction cycle represented by the following chemical equations:[54]

$$E+H_2O_2 \rightarrow E\text{-}I+H_2O$$

$$E\text{-}I+AH_2 \rightarrow E\text{-}II+AH\cdot$$

$$E\text{-}II+AH_2 \rightarrow E+ AH\cdot+H_2O$$

where E is the native KatG, E-I and E-II are active KatG compound I and II, respectively, AH_2 is a reducing substrate such as 2-naphthol, aniline and $AH\cdot$ is a free radical product. The overall reaction can be described as $2AH_2+H_2O_2 \rightarrow 2AH\cdot+2H_2O$.

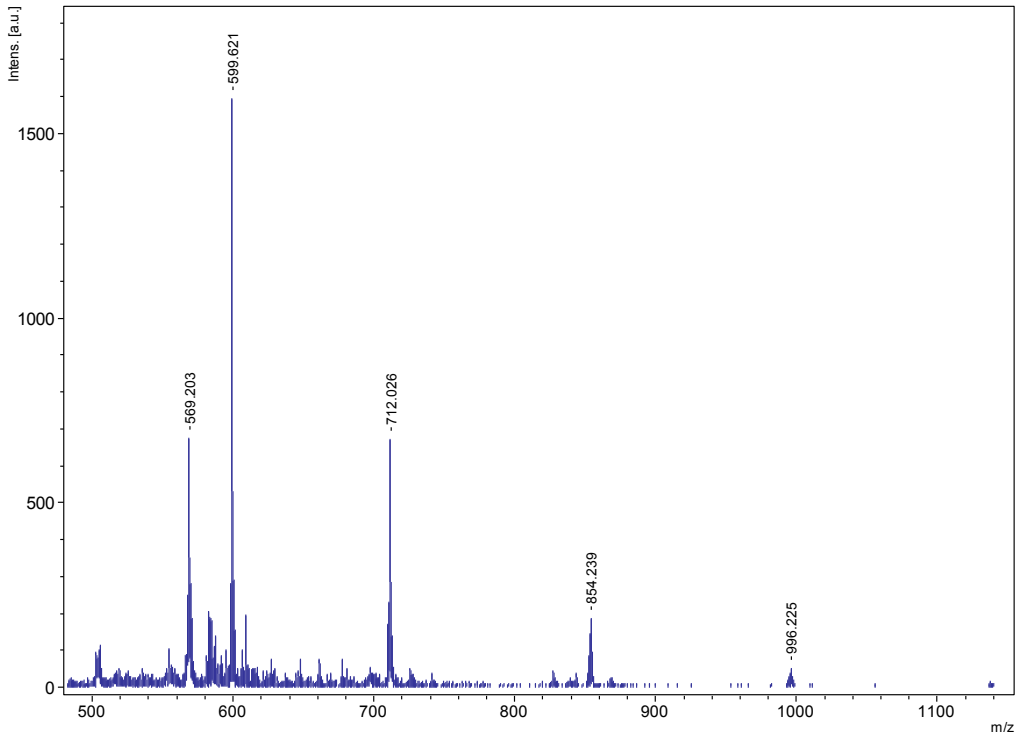

Figure 2-9 MALDI - MS Data for the 2-naphthol polymerization product after 25 mM H_2O_2 and 1 mM of 2-naphthol with 1 µl KatG-bound chip left for 1 h

As shown in Figure 2-8 and 2-9, the free radical products readily undergo self-coupling with other radicals in solution through nucleophilic addition. This results in the formation of larger oligomers. Furthermore, radical products can facilitate the cross-coupling reactions via phenoxy-radicals.

2.4 Conclusion

Herein we have shown that 2-naphthol polymerization can be achieved by oxidative polymerization of 2-naphthol, catalyzed by surface-bound Y559(DOPA) mutant KatG. This reaction can be widely used as a treatment method for a variety of phenolic

contaminants in water, waste water and soils. Our attempt to characterize 2-naphthol products using mass spectroscopy (MALDI) was successful as we have seen the oligomers formed coupling through C-C and C-O or C-O-C bonds. Hence, bead-bound KatG can be developed as an environmental remediation technique for phenolic contaminated water.

Chapter 3

Investigation of pH and Surfactants Effect for Immobilized Y559(DOPA) Mutant KatG with H_2O_2

All the experiments in this chapter were done by Yanbo Zhang in the laboratory of Prof. Roshan Perera.

3.0 Introduction

H_2O_2 has various applications in medical devices. It is approved to be used by FDA in many medical device manufacturing applications and also classified as an antimicrobial agent.[55-58] H_2O_2 has a powerful disinfection efficacy and therefore, can be used as a disinfecting solution.[59-60] It can be used as a bleach agent and has been used to sterilize the biological safety cabinets, artificial satellites and space probes and also as a propellant in rocketry. H_2O_2 is a highly effective contact lens care solution at killing pathogens, including fresh water amoeba which causes diseases in humans.[57]

As a powerful oxidizer than chlorine, chlorine dioxide and potassium permanganate, H_2O_2 generates a highly reactive oxygen species (ROS). ROS can cause toxic effects on all the components in cells, like lipids, DNA, proteins, through the production of peroxides. Excess H_2O_2 produced as a by-product of oxidative metabolism intensifying the oxidative stress in biological systems can be decomposed naturally by catalases. However, undecomposed H_2O_2 in disinfecting solutions create problems as irritations, inflammations, and swelling in contact with the human skin. Therefore, the development of a powerful, user-friendly neutralizing agent is in high demand to eliminate the undecomposed H_2O_2 remaining in solutions.

Inorganic catalysts, including manganese dioxide (MnO_2), silver (Ag), and platinum (Pt) based catalysts are some favorite molecules for neutralizing H_2O_2. Most commonly used catalyst in market is Pt-based catalyst. The major problems for these products are that:

(1) Pt catalysts are expensive

(2) Contaminate the medical devices

(3) The neutralization process doesn't last long

(4) Hard to immobilize on the surface (leach off)

(5) Decompose H_2O_2 before sterilization completes

Obvious green solution for this issue is catalase-based sterilizing agent. Catalase is present in virtually all aerobic organisms and many anaerobic organisms including humans and is well known to decompose H_2O_2 to dioxygen and water. The extensive sequence homology and structural similarity suggested that many of the properties of these enzymes would be similar. But studies have revealed just the opposite; there are striking variations of 10 to 1000 times in specific activities, reaction velocities, sensitivity to damage by the substrate H_2O_2, and sensitivity to inactivation by inhibitors and heat. For example, commercial 3% H_2O_2 can have 850 mM to 1100 mM concentration of H_2O_2. At such a high H_2O_2 concentrations, small-subunit catalases exhibit lower velocities because of inactivation by H_2O_2.

Furthermore, once inactivated, catalase needs reduced NADPH cofactor to prevent accumulation of inactive compound II (Figure 4-1). Therefore, an extensive supply of NADPH is required to decompose the excess H_2O_2, due to the fact that catalase activity depends on the reduced form of NADPH cofactor.[61-62] Oxidization of NADPH in the presence of high H_2O_2 concentration (~1.5%) leading to the inactivation of catalase, however, limits all its possible practical applications. Furthermore, free catalase protein left on the contact lenses after H_2O_2 sterilization generates side effects.

In order to address these disadvantages mentioned above, a novel strategy has been developed in this chapter using KatG. KatG, a bifunctional enzyme secreted by *Francisella tularensis*, exhibits both catalase and peroxidase activity. Different from monofunctional catalase, the catalase activity of KatG is not NADPH-dependent and it exerts potent catalase activity in the presence of high 3% H_2O_2 concentration which enables its ample practical applications over catalase.

In previous chapter, I have explained the immobilization technique for the DOPA KatG mutant enables protein anchoring to the solid surface, resulting in no escape of the free protein to the disinfecting solutions. $NaIO_4$ mediated bioconjugation is employed in this study and will facilitate the native binding of Y559(DOPA) KatG to the amine-derivatized surface in the presence of DOPA quinone on the protein surface (Chapter 2).

Delayed decomposition for peroxide solution is of vital importance in contact medical device disinfections. However, neutralizing agents in the market now have various problems, like inefficient at high concentration of H_2O_2, free protein contamination, coating material dissolution, etc. Herein we propose a greener, high-impact, highly efficient and cost-effective strategy to develop a sterilizing agent.

In this chapter, a greener strategy has been introduced. We have divided this chapter into three main objectives. The first objective will address the delayed decomposition technology for peroxide solution chemistry. Instead of using the catalase, a catalase-peroxidase (KatG) is used. Secondly, in order to overcome the contamination problem of the medical devices (the free proteins released in solutions) during the H_2O_2 decomposition, Michael addition reaction based immobilization technique has been employed in the experimental design. The immobilization of native proteins on a solid surface will achieve the goal of maximum retention of activity, structural integrity (preserving the secondary and tertiary structures of proteins) and no escape of free

protein into disinfecting solutions. Thirdly, by using buffered H_2O_2 solutions at varying pHs (5.5 to 7.5) we have established the performance of Y559(DOPA) mutant KatG. Finally, we have also tested surfactant effect for the immobilized KatG.[63-68]

3.2 Materials and Methods

3.2.1 *Protein Immobilization onto Surfaces*

$NaIO_4$ mediated bioconjugation reaction was carried out in Y559(DOPA) mutant KatG in Kphos buffer at pH 6.0 for 2h gentle shaking at room temperature.

3.2.2 *Potassium Permanganate Titration with H_2O_2*

100 µL of 3% H2O2 solution (with different formulations) after each the scale during neutralization was taken to titrate with 10 mM Potassium permanganate at different time intervals.[69]

$$5\ H_2O_2(aq) + 2\ MnO_4^-(aq) + 6\ H^+(aq) \rightarrow 2\ Mn^{2+}(aq) + 5\ O_2(g) + 8\ H_2O(l)$$

3.3 Results and Discussion

It can been vividly seen oxygen bubbles were produced and released constantly from the 3% hydrogen peroxide solution with the catalysis of Y559(DOPA) KatG tagged glass beads (Figure 3-1).

Figure 3-1 Oxygen bubbling Y559(DOPA) KatG-bound glass bead in H_2O_2

Covalent attachment prevented the leaching of Y559(DOPA) KatG to the H_2O_2 solution based on the fact that oxygen bubbles were generated only from the glass beads.

3.3.1 *Kinetics of Covalently Immobilized Y559(DOPA) KatG Neutralizing a H_2O_2 Solution*

To investigate the practicability of the covalently immobilized DOPA KatG as a neutralizing agent for a H_2O_2 solution, a series of formulations were based on the pHs and surfactants. The efficacies of neutralizing 3% H_2O_2 among two widely-used neutralizers available in market and Y559(DOPA) KatG tagged glass beads have been compared (Figure 4-3). Neutralizer 1 is a Platinum catalyst product, while neutralizer 2 is a catalase tablet. As seen in the titration curves, neutralizer 1 dramatically reduced the concentration of H_2O_2 from 3.3% to 0.8% within 20 min. surprisingly, no more consumption of H_2O_2 was observed during the following 70 min. exposure time. Similar to the fast neutralization in neutralizer 1, in the first 20min., neutralizer 2 dropped the

concentration of H_2O_2 from 3.4% to 1.5%. However, it succeeded to remove almost all the H_2O_2 within 90 min. Such result can be explained by the deactivation of the protein, due to oxidation of NADPH and heme bleaching. Lack of long enough exposure for the device to at least 1% H_2O_2 solution in these two neutralizers failed to ensure the disinfection against a broad range of microorganisms. Obviously, superior disinfection efficacy results from prolonged contact lenses exposure to 3% H_2O_2 before neutralization begins. In contrast to these two neutralizers, Y559(DOPA) KatG -bound glass beads/silica delayed the neutralization process to prolong the disinfection. In the beginning 20 min., they both showed almost the same neutralizing rate as the above mentioned two neutralizers. But in the following 70 min., the neutralizing rates decreased to approximately half of their rates of the first 20 min. within 5h, total decomposition of H_2O_2 has been observed. Hence, it can be concluded that covalently immobilized Y559(DOPA) KatG overcome the disadvantages regarding the exposure time to H_2O_2 and has proven to be a powerful decomposition agent for 3% H_2O_2.

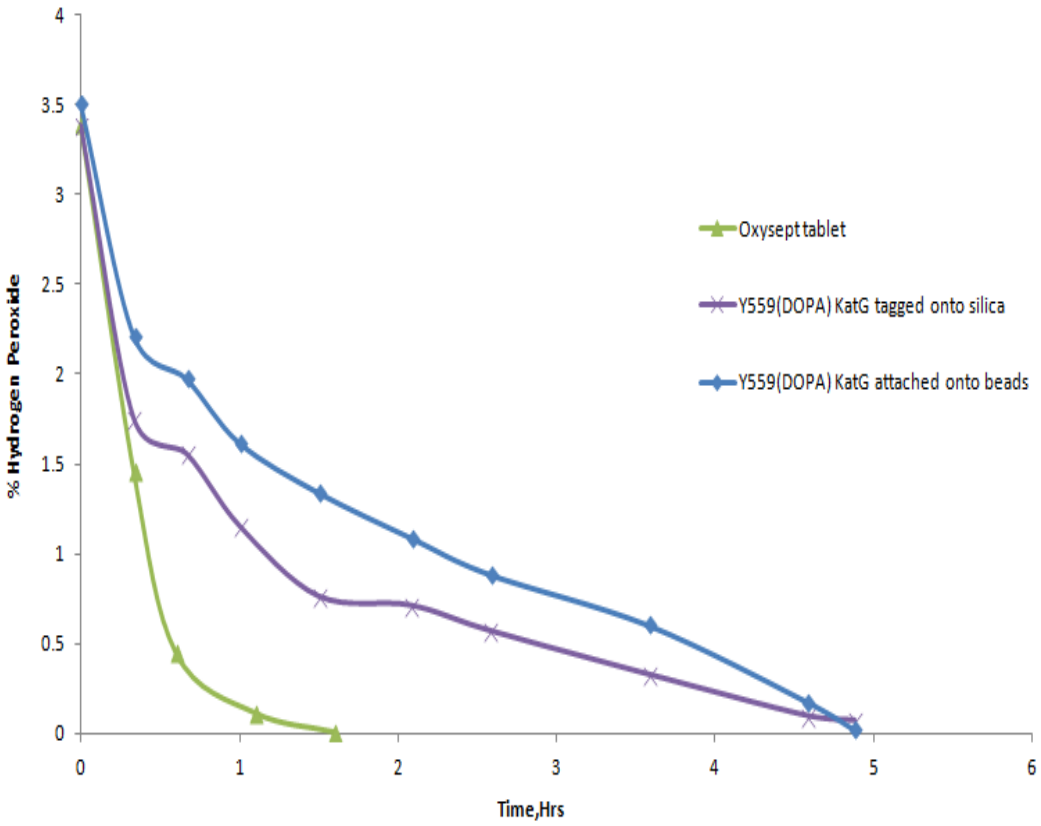

Figure 3-2: Potassium permanganate titration data of a 3% H_2O_2 vs. time. Oxysept is a current free catalase in the market.

In addition for the development of this method another method has been done using the plastic based tablet (with immobilized protein) neutralization of 3% H_2O_2 solution as shown in Figure 3-3.

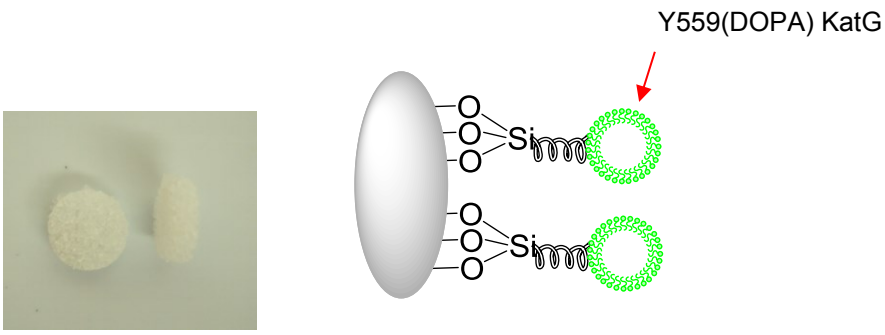

Figure 3-3 Y559(DOPA) KatG-bound plastic tablet

The results displayed prolonged neutralization suggests that the tablet design can be carried out successfully in a cost effective way. At the same time the tablet coverage of the protein can be altered to achieve the preferred neutralization data. Figures 3.4 and 3-5 display decomposition of 5 different plastic tablets and their ability to use in a consistent fashion. By modifying the concentration of the protein in the reaction mixture during attachment can also give some control over the immobilization within shorter error margin as indicated in the plot with error bars with standard errors for 5 different data sets collected for 5 separate tablet-bound proteins (Figure 3-5).

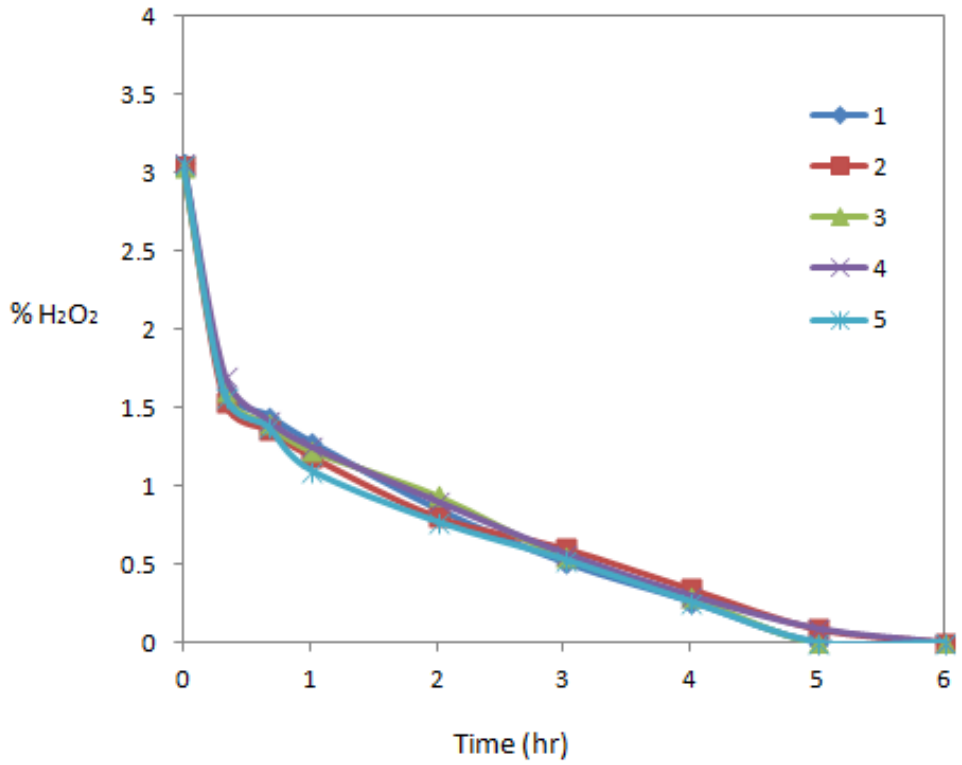

Figure 3-4: Average plot for titration data (five different data sets based on 5 tablets) based on plastic tablet with immobilized protein for a 3% H_2O_2 solution.

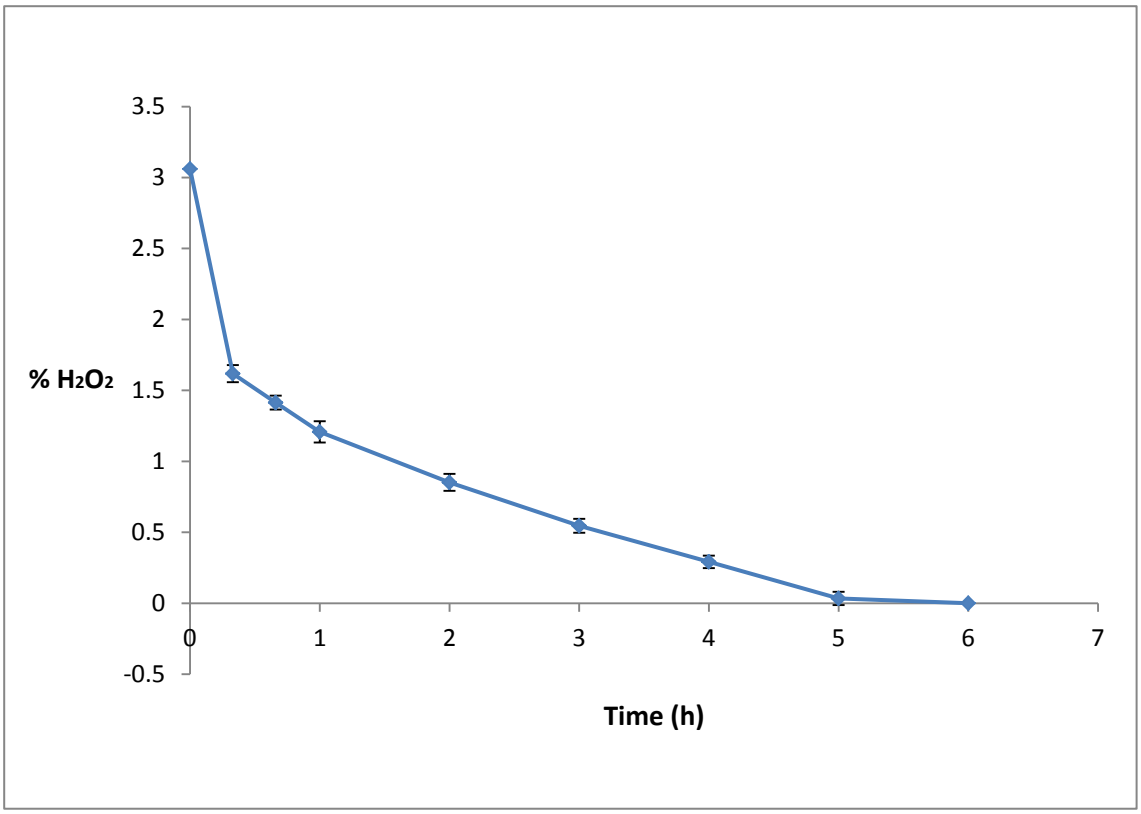

Figure 3-5: Titration data (five different data sets based on 5 Y559(DOPA) KatG immobilized plastic tablets) with standard error bars.

.

Objective 1: Neutralization and temperature studies of immobilized Y559(DOPA) KatG as a function of time.

Formulations tested:

A-1: 3% H_2O_2 vehicle (no surfactant) - pH 6.5

A-2: 3% H_2O_2 vehicle (no surfactant) - pH 7.0

A-3: H_2O_2 vehicle (no surfactant) - pH 7.5

(A)

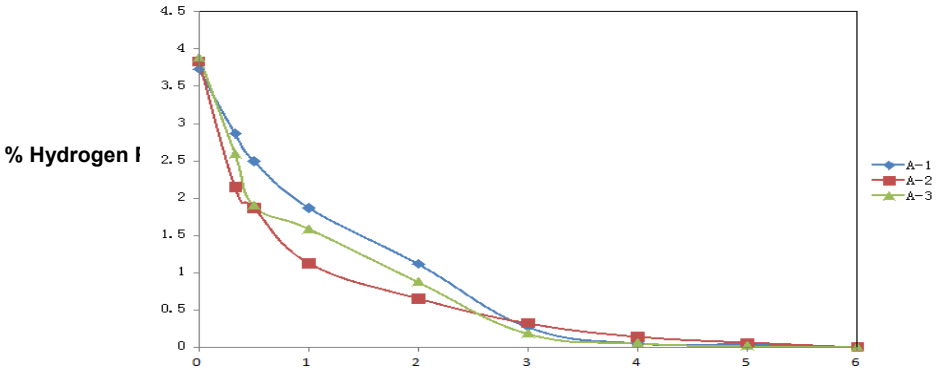
% Hydrogen I
4.5
4
3.5
3
2.5
2
1.5
1
0.5
0
0
1
2
3
4
5
6
A-1
A-2
A-3

(B)

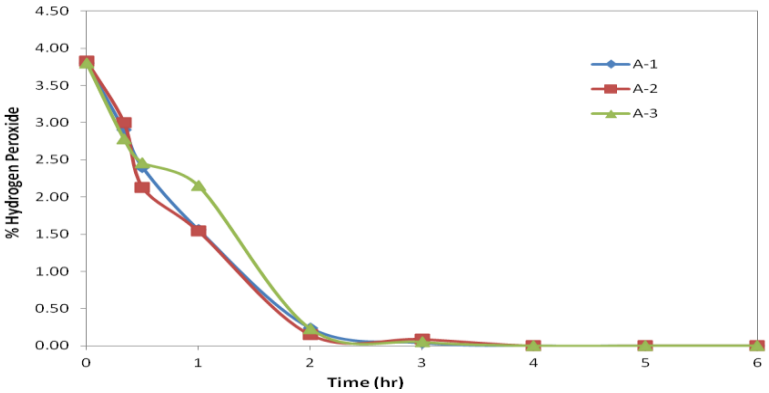
% Hydrogen Peroxide
4.50
4.00
3.50
3.00
2.50
2.00
1.50
1.00
0.50
0.00
0
1
2
3
4
5
6
Time (hr)
A-1
A-2
A-3

(C)

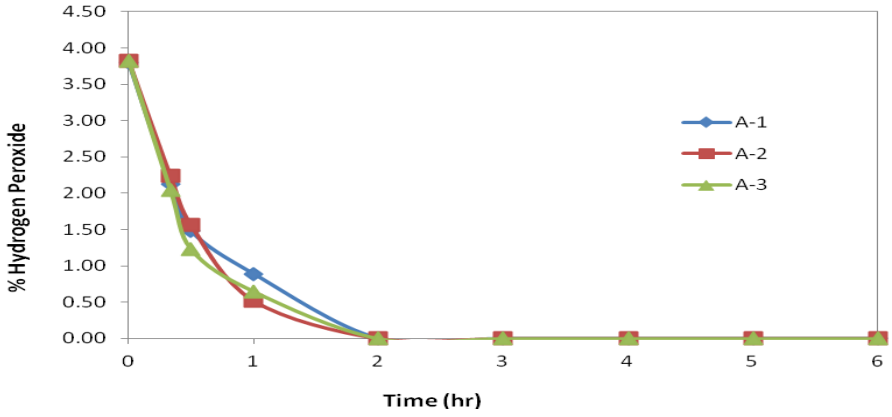
% Hydrogen Peroxide
4.50
4.00
3.50
3.00
2.50
2.00
1.50
1.00
0.50
0.00
0
1
2
3
4
5
6
Time (hr)
A-1
A-2
A-3

Figure 3-6: (A) Temperature and neutralization titration data (3 different data sets based on 3 formulations) based on plastic tablet with immobilized protein at 4 ºC; (B) Titration data (3 different data sets based on 3 formulations) based on plastic tablet with immobilized protein at 25 ºC; (C) Titration data (3 different data sets based on 3 formulations) based on plastic tablet with immobilized protein at 45 ºC.

All titration curves were averaged with 3 trials. These three figures showed stability with temperature. However, the durability of Y559(DOPA) KatG immobilized plastic tablets in 3 different formulations with three pHs (6.5, 7, 7.5) at three different temperatures did not show repeatability beyond two times usage. It is noticed that at the elevated temperature, the Y559(DOPA) KatG immobilized tablets still showed the neutralization activity. It can be concluded there is no risk of protein denaturation at exposure to this condition.

Objective 2: Evaluate surfactant effects on immobilized catalase activity

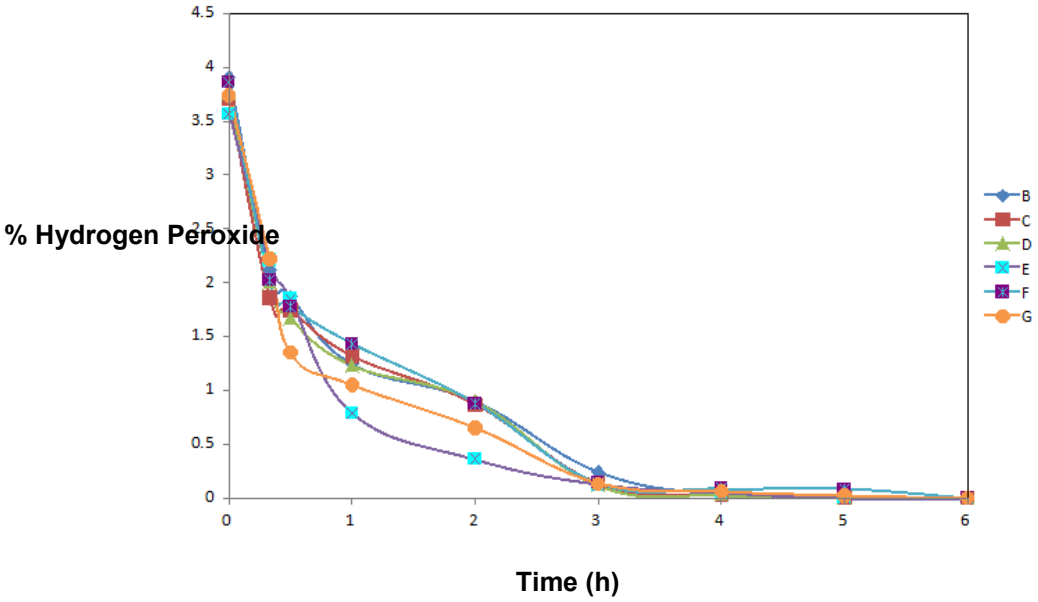

Figure 3-7: 6 different titration data (averaged out from 3 data sets) sets based on plastic tablet with immobilized protein for 6 formulations B-G with different surfactants (pluronic and AL-91181).

Formulations tested:

B: H_2O_2 vehicle (no pluronic 17R4) - pH 6.5

C: H_2O_2 vehicle + 0.05% pluronic 17R4 + - pH 6.5

D: H_2O_2 vehicle + 0.05% pluronic 17R4 + 0.12% AL-91181 - pH 6.5

E: H_2O_2 vehicle + 0.05% pluronic 17R4 + 0.04% AL-91181 - pH 6.5

F: H_2O_2 vehicle + 0.05% pluronic 17R4 + 0.08% AL-91181 - pH 6.5

G: H_2O_2 vehicle + 0.04% AL-91181 (no pluronic 17R4) - pH 6.5

Surfactants effects have been evaluated in 6 formulations with various surfactants from Pluronic family and nEOBO lead.[66,68,70] For each test group, 3 trials have been carried out and these three data sets were averaged out to plot in the titration curves above. As seen on the titration curves, Y559(DOPA) KatG immobilized tablets' activity is not at all affected by the surfactants.

Objective 3: Effects of post-H_2O_2 neutralization storage (durability) conditions on catalase activity.

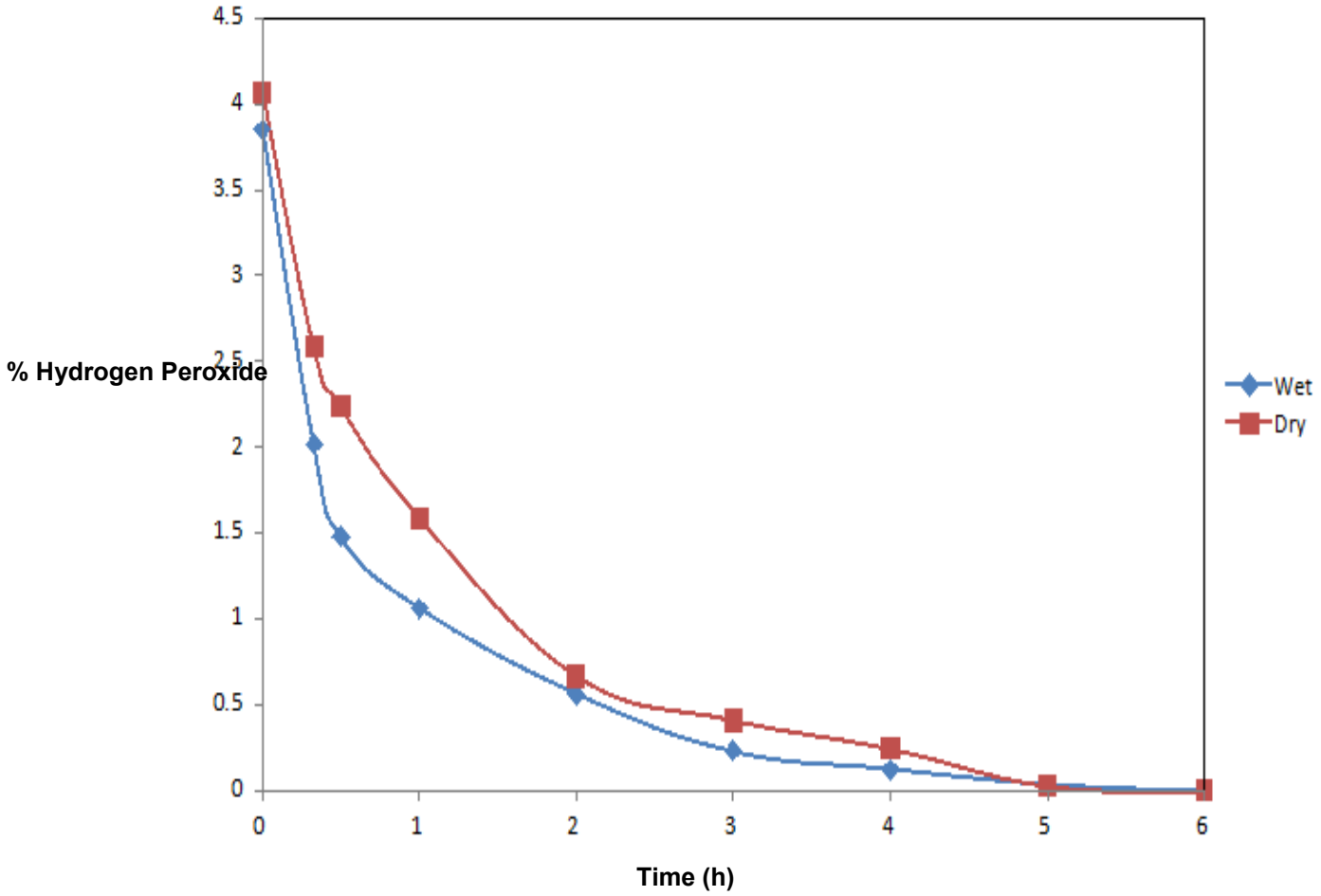

Figure 3-8: 3 different titration sets averaged plots based on plastic tablet with immobilized protein for the formulation B under the dry and wet storage conditions.

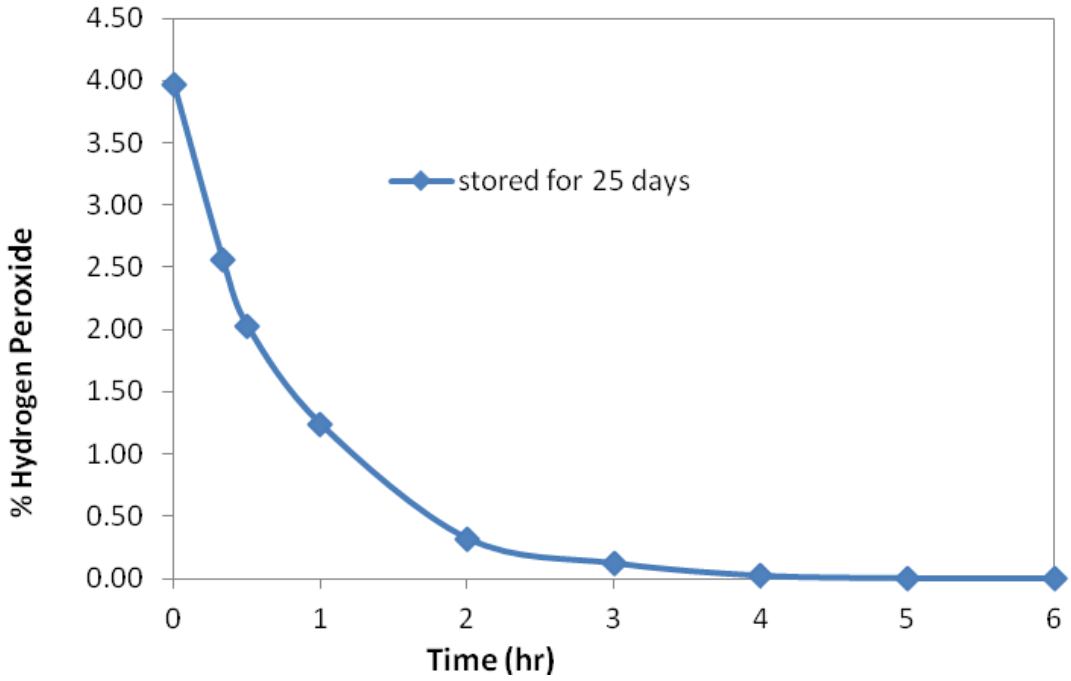

Figure 3-9: Three averaged titrations based on plastic tablet with immobilized protein stored for 25 days (dry) for the formulation B.

In this study, the effects of storage conditions have been investigated. For the "wet" titration, between the cycles, Y559(DOPA) KatG immobilized tablets were stored in neutralized solution for overnight. The titration curve was averaged with 3 trials. For the "dry" titration, Y559(DOPA) KatG immobilized tablets were kept in the air-dry condition overnight before initiation of the next cycle. From the titration curves, it proves that our Y559(DOPA) KatG immobilized tablets can sustain a good reproducibility as found in fresh ones.

Objective 4: Evaluate surface area vs. activity as a function of surface area of immobilization.

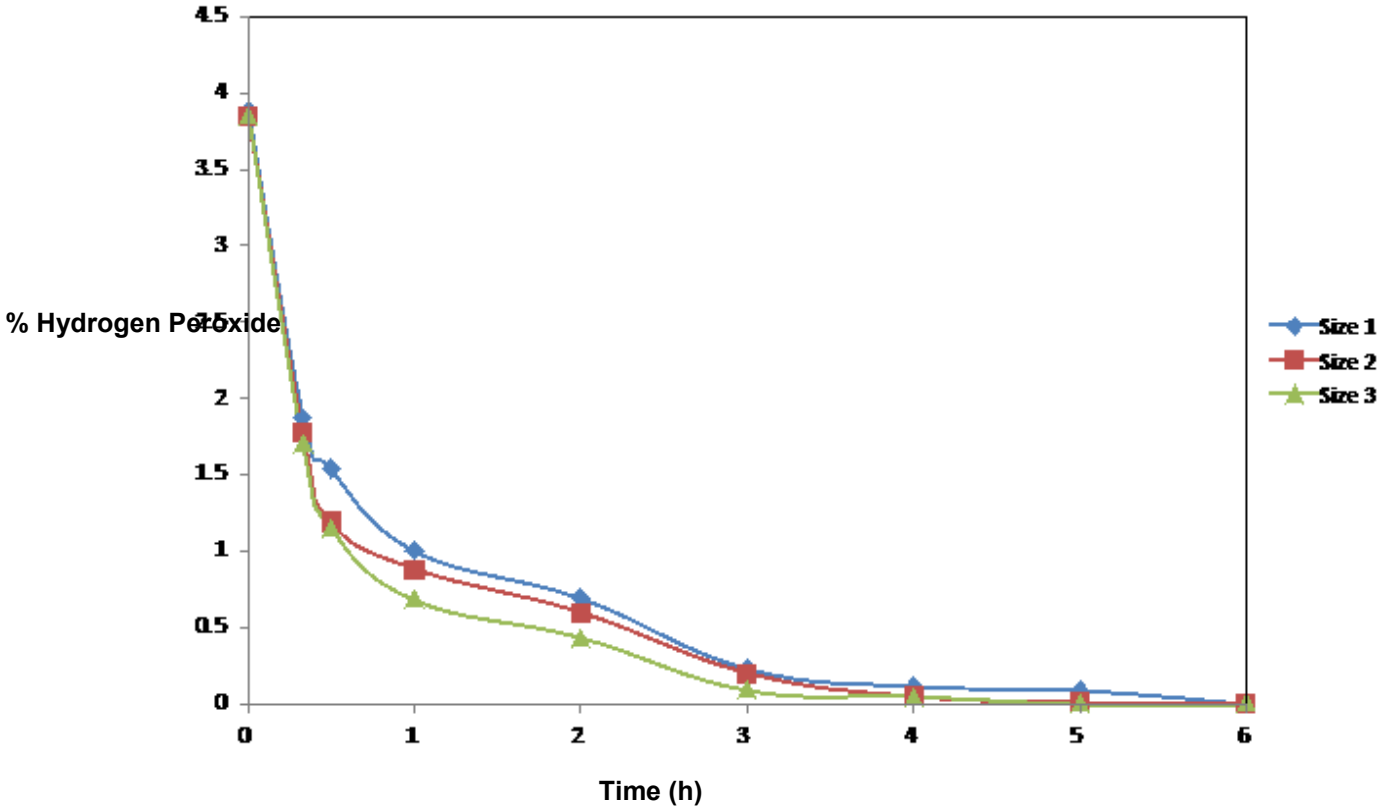

Figure 3-10: 3 different titration sets based on plastic tablet with immobilized protein on 3 different surface areas for the formulation B. (Surface area of size 1: 1.28 cm^2; Surface area of size 2: 1.90 cm^2; Surface area of size 3: 3.16cm^2.)

The Y559(DOPA) mutant KatG was immobilized onto three different sized tablets and titrated for its neutralization ability. Size 1and 2 showed a better titration capacity than size 3 which gave a much faster H_2O_2 consumption rate.

3.4 Conclusion

In conclusion, I compiled the H_2O_2 decomposition data to carry out 3% H_2O_2 neutralization without free proteins or chemicals in solution. Furthermore, our method has increased the duration of neutralization (delayed neutralization ensures superior disinfection efficacy) and completed removal of H_2O_2 after prolong exposure.

Chapter 4

Generation of Novel Features via Unnatural Amino Acids Incorporation into the Enhanced Green Fluorescence Protein (EGFP)

All the experiments in this chapter were done by Yanbo Zhang in the laboratory of Prof. Roshan Perera.

4.1 Introduction

Fluorescence proteins have been used extensively in life sciences for imaging and labeling work, and therefore of a great importance.[71-74] They are used as fluorescence markers in protein labeling to study the location of the protein of interested *in vivo*.[75-76] As a noninvasive biomarker, it can also be applied in monitoring gene expression, detection of protein-protein interactions, and genetically encoded sensors (Fluorescent proteins as a toolkit for *in vivo* imaging).[77-78] Green fluorescent protein (GFP) was first isolated from jellyfish *Aequorea victoria.* Attention was not attracted until *gfp* gene was first cloned and expressed in bacteria. Various GFP mutants were created to be widely used in molecular biology, with enhanced fluorescence, different spectroscopic features or improved conformational stability.[79]

The interesting property of aquaria EGFP is that the chromophore inside the protein cylinder is an integral part of EGFP peptide chain originating from Ser65-Tyr66-Gly67 sequence, which involves the post-translational modification of fast nonenzymatic cyclization between Ser65 and Gly67 and following rate-limiting O_2 oxygenation (around 4 hours) of the Tyr 66 to form a 4-(*p*-hydroxybenzylidene)-imidazolidin-5-one structure (Figure 5-1).[80]

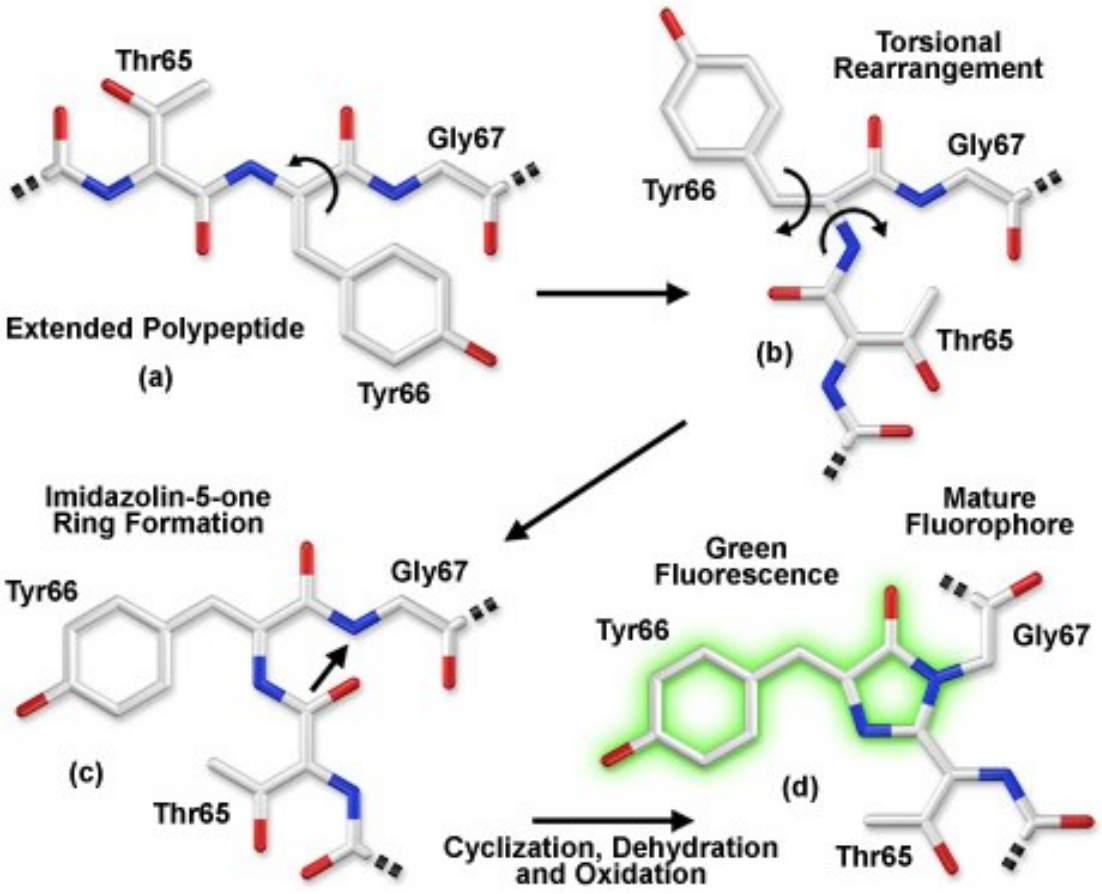

Figure 4-1: Structure of the GFP chromophore.

Since in enhanced green fluorescent protein (EGFP) Tyr 66 was mutated to lysine residue to increase the green luminescent color, this suggests that by mutating residues within this protein color chromophore can be further modified.

The genetic incorporation of unnatural amino acids (UAAs) into proteins has proven to be a powerful technique for adding extra functional properties into proteins in their native conformation. For example, the ability to introduce 3-aminotyrosine (3-NH_2Tyr) amino acid at defined sites in proteins would give an opportunity to carry out a

formation of a strong permanent linkage (Diels-Alder reaction) with the acrolyl derivatized solid support.[81] On the other hand, 3,4-L-dihydroxyphenylalanine (DOPA) can facilitate the Michael addition reaction with amine groups on the surfaces. Hence, we were curious that by replacing the amino acids with UAA in the active center of the protein, for instance, in the vicinity of the chromophore in EGFP, will significantly affect its new and enhanced color chromophore properties in both wavelength shifts and intensity, enabling a rational way to expand the fluorescence spectrum through amino acids substitution.[71,82-85]

Our EGFP amino acid analysis shows that there are nine tyrosine amino acid residues at position 39,74,92,106,143,145 (adjacent to the chromophore),151,182,and 200 (PDB accession number 1Z1P). In this study, we have selected Selective Pressure Incorporation (SPI) method to incorporate and replace all these tyrosine amino acid residues with L-DOPA or $3NH_2$Tyr.[86] Unnatural functionalization of proteins can be achieved through pure chemical approaches like chemical modifications and total artificial synthetic genes of small proteins generating hybrid variety via gene expression.

4.2 Materials and Methods

4.2.1 *Materials*

Arabinose was purchased from Sigma. *E. Coli* strain JW2581 tyrosine anxotroph competent cells were obtained from The Coli Genetic Stock Center,Yale University.

4.2.2 *WT EGFP and Mutant EGFP Expression and Purification.*

WT EGFP with N-term 6xHis tag added to EGFP gene in *E. Coli* DH10B expression host was grown at 37 ^{0}C in Luria-Bertani (LB) broth containing 100 μM

Ampicillin until OD_{600} value reached ~0.8. 20% Arabinose was then added to induce the WT EGFP expression for 8h at 30 ^{0}C. Cells were harvested by centrifugation and lysed in lysis buffer (50 mM Tris,100 mM NaCl,pH 8.0). The protein is purified under native conditions. The cell suspension was treated with 80 µL Lysozyme (100 mg/mL), 40 µL DNase I (5 mg/mL) and 40 µL of RNase A (100 mg/mL). The cell suspension was stirred at 4 ^{0}C for 1h to allow lysis to occur. The clear supernatant after 1h centrifugation at 9,000 rpm, in 4 ^{0}C was loaded onto a nickle nitroloacetic acid resin (Qiagen,Hilden,Germany) and eluted to afford ~10 mg/L of protein.

4.2.3 *Tyr*(9) DOPA or 3NH_2Tyr EGFP Mutants*

SPI method was used to express mutant EGFP by replacing all the 9 tyrosine residues with UAAs, either 3,4-Dihydroxy-L- phenylalanine (DOPA) or 3-aminotyrosine (3-NH_2Tyr). EGFP-pBAD plasmid was transformed into *E.Coli* JW2581 tyrosine anxotroph competent cells. The transformed cells were grown in M9 minimal media containing 0.4% (w/v) of glucose, 0.1 mM $CaCl_2$, 1.0 mM $MgSO_4$, 35µg/mL thiamine, 40 mg/L 20 L-amino acids, 100 µM *Ampicillin* and 100 µM *Kanamycin* until OD value reached 1.0. Cells were then centrifuged for 10 min at 5,000 rpm in 4 ^{0}C. The cell pellets were washed twice with 0.9 % (w/v) NaCl solution. Then the cells were resuspended in M9 minimal media containing 19 L-amino acids (however in the absence of tyrosine), instead either 1 mM DOPA or 1 mM 3NH_2Tyr was added, other components were the same. After 10 min shaking at 37 ^{0}C, 0.2 % Arabinose was added to induce the mutant EGFP expression for 8h at 30 ^{0}C. The following steps were the same as WT EGFP expression and purification.

4.2.4 *Protein Immobilization onto Derivatized Glass Surface*

The Diels-Alder reaction was employed in nine 3NH_2Tyr-incorporated EGFR mutant immobilization to form a strong permanent linkage with the solid support-

containing acrylic group just by adding 200 μM sodium per-iodate on glass or silica beads. DOPA containing proteins will initiate the Michael addition reaction with amine groups during protein attachment on to the surface using sodium per-iodate. Functionalization of the glass surface for these reactions has been described in Chapter 2.

(A)

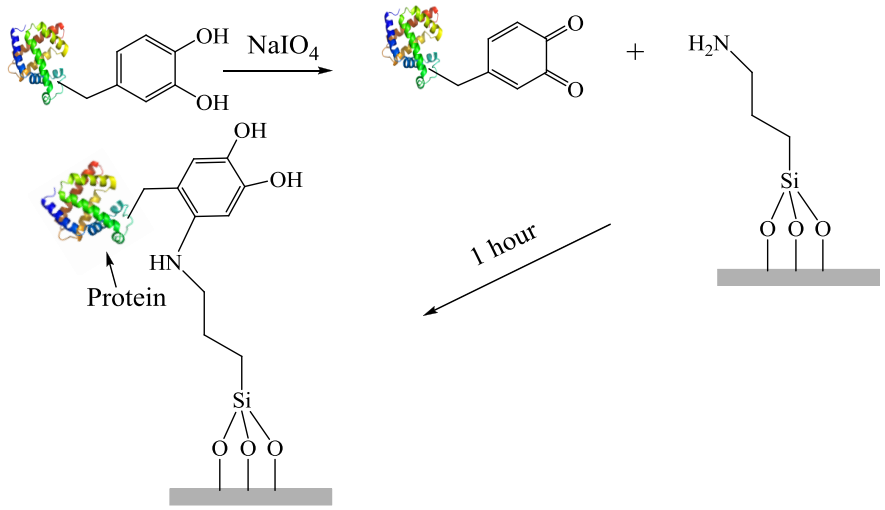

(B)

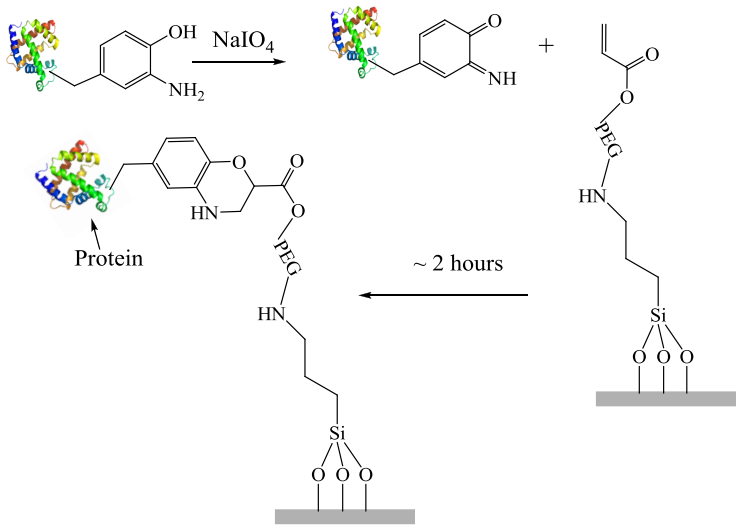

Figure 4-2: Schematic representations of (A) Michael addition reaction in DOPA-containing EGFP; (B) the Diels-Alder reaction in $3NH_2$Tyr-containing protein EGFP protein[81]

4.2.5 *Atomic Force Microscope (AFM) Imaging*

Veeco MultiMode V SPM performed the surface topography of EGFP wild type and mutants tagged amine-functionalized glass slide.

4.3 Results and discussion

Table 4-1. GFP Tyr residues in the amino acids sequence:

Y* = DOPA or $3NH_2$Tyr
10 20 30 40
GFP MSKGEELFTG VVPILVELDG DVNGHKFSVR GEGEGDATNG
50 60 70 80
GFP KITLKLICTT GKLPVPWPTL VTTCG**Y***GVQC FAR **Y***PDHMKR
90 100 110 120
GFP HDFFKSAMPE G **Y***VQERTISF KDDGTFKTRA EVKFEGDTIV
130 140 150 160
GFP NRIKLKGIDF KEDGNILGHK LE **Y***NFNSHNK **Y***ITADKQKNG
170 180 190 200
GFP IKANFKIRHN VEDGSVQLAD H **Y***QQNTPIGD GPRLLPDNH **Y***
210 220 230
GFP LSTQSVILED PNEKRDHMVL HEFVTAAGITHGMDEL **Y***K

The detailed sequence information about the EGFP variant used in the study was mentioned in Table 4-1. Glass chip surface was selected for the bioconjugation reaction. In this study we expressed our recombinant protein EGFP by replacing all 9 tyrosine residues with unnatural amino acid DOPA or 3-NH_2Tyr. Cells containing recombinant EGFP were expressed in minimal medium containing the 19 amino acids only (without tyrosine). Since, oxidation of DOPA and 3-NH_2Tyr lead to the formation of highly reactive quinone and amino quinone moieties, respectively, which are believed to induce toxicity in the cell. We suspected that the toxicity may affect the protein expression level in the cells. Therefore, to prevent the oxidation of DOPA and 3-NH_2Tyr, the EGFP mutants were expressed in the minimal medium under slightly acidic conditions (pH=6.5).

After the expression, crude bacterial lysate was run on a SDS-PAGE gel (as shown in Figure 4-3) to analyze the expression level. Based on the gel, the mutants expression level is comparable to that of WT EGFP. It suggests that the expression protocol is a success.

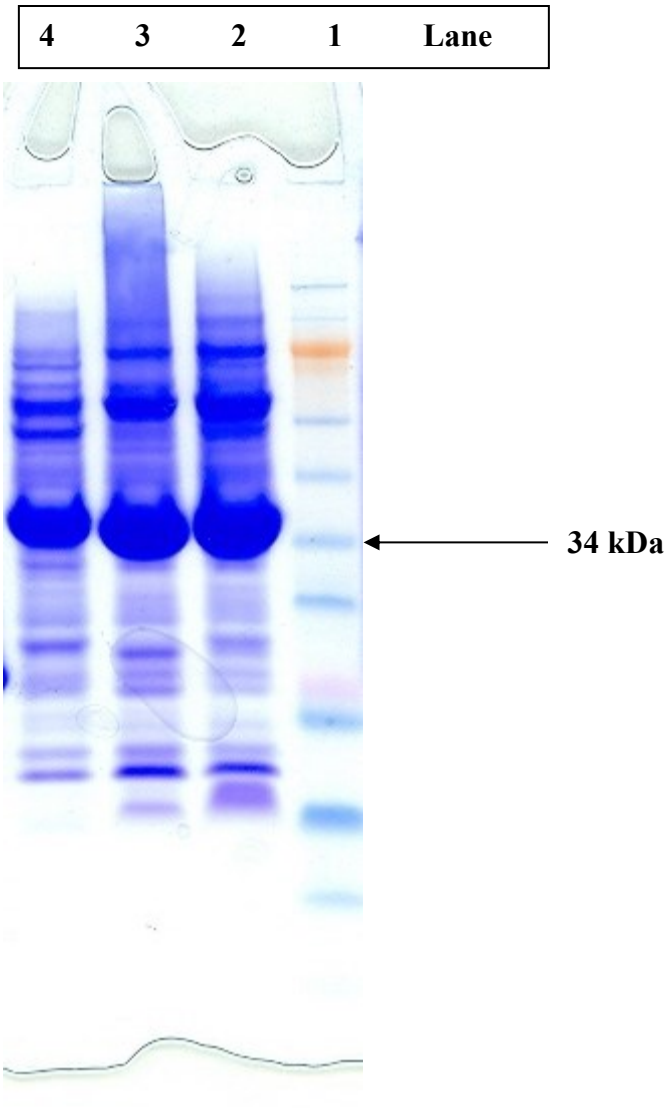

Figure 4-3: SDS-PAGE gel for the crude cell lysate of the express EGFP. Lane 1: the protein ladder; Lane 2: EGFP with all 9 Tyrosine replaced by 3-NH_2Tyr; Lane 3: EGFP with all 9 DOPA replaced by 3-NH_2Tyr; Lane 4: wild-type EGFP.

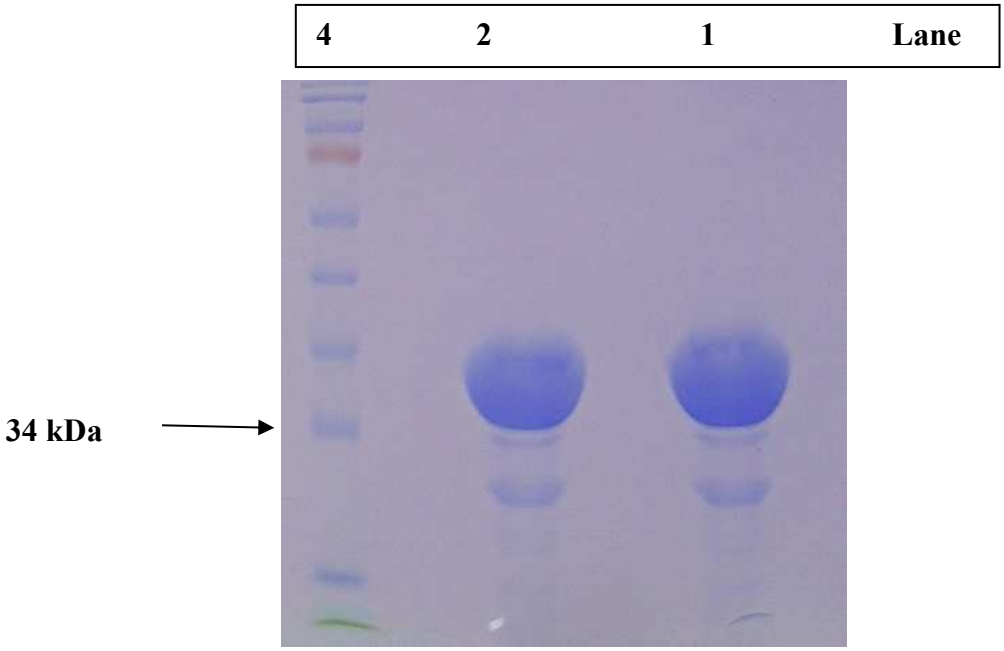

Figure 4-4: Coomassie-stained SDS-PAGE analysis of EGFP. Lane 1: EGFP with nine 3-NH_2Tyr amino acids; Lane 2: EGFP with nine DOPA amino acids

4.3.1 *Atomic Force Microscope (AFM) Imaging*

AFM topography was used to visualize the protein arrays on the derivatized glass surface. As seen in the images, Both mutants show quite large amount of protein tagging onto the surface compared to the control.

DOPA*-9 and 3-NH_2Tyr*-9 EGFP protein Figure 5-5-(A) shows an average height of 25 nm for the DOPA*-9 and 3-NH_2Tyr*-9 EGFP which is consistent with the size of the

protein based on the crystal structure of the wild-type EGFP. Figure 5-5-(B) corresponds to the acryloyl derivatized glass slide.

Though the immobilization reaction for DOPA*-9-EGFP and $3NH_2$Tyr*-9 EGFP could be random, there is some uniformity of the reaction. It seems like that the is no bioconjugation happened during immobilization (can not 100% confirms this with AFM). However, it can be confirmed that wild-type EGFP (after the treatment with 200 μM $NaIO_4$, did not show significant binding as shown in Figure 5-5 (C). Except the orientation of the protein, the effective tagging can be confirmed with these AFM data. By immobilizing mutants EGFR on the surface, we have shown that they indeed have UAAs in them. Otherwise, there will be no possibility (like in wild-type case) for them to bind to the glass surface with the Diels-Alder reaction or the Michael addition reaction.

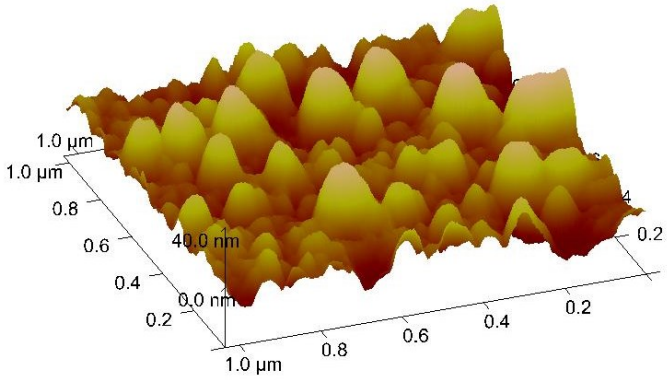
1.0 µm
1.0 µm
0.8
0.6
40.0 nm
0.4
0.0 nm
0.2
0.2
1.0 µm
0.8
0.6
0.4
0.2

(A)

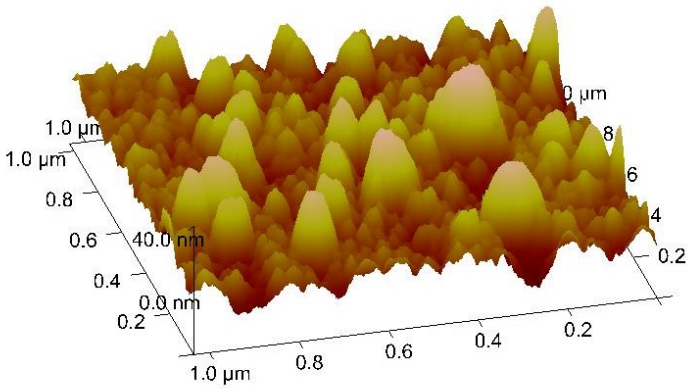
1.0 µm
1.0 µm
0.8
0.6
40.0 nm
0.4
0.0 nm
0.2
0.2
1.0 µm
0.8
0.6
0.4
0.2

(B)

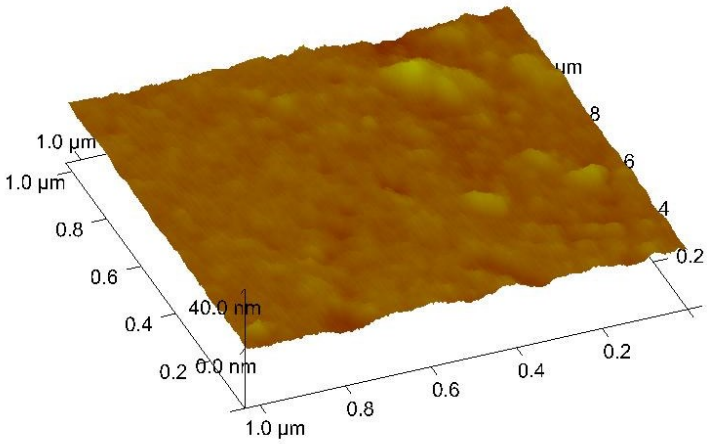
1.0 µm
1.0 µm
0.8
0.6
40.0 nm
0.4
0.0 nm
0.2
0.2
1.0 µm
0.8
0.6
0.4
0.2

(C)

Figure 4-5: Three dimensional representation of the AFM images for (A) Tyr* 9-DOPA EFGP attachment to an amine functionalized surface; (B) Tyr* 9- 3NH_2Tyr EFGP EGFP attachment to an acryloyl functionalized surface; (C) Control: WT EGFP

4.3.2 *Color Change of EGFP through DOPA or 3-NH_2Tyr Replacing All 9 Tyrosines*

While WT EGFP giving a greenish color, EGFP with nine DOPA shows an intense brown to reddish color. However, EGFP with nine 3-NH_2Tyr shows a less intense reddish color. DOPA containing EGFP's color change might be due to one additional hydroxy group in 145 position in the side chain with close contact to the chromophore. Likewise, the color difference of 3-NH_2Tyr containing EGFP might result from one additional amino group at position of 145. There could be several other reasons for this change, such as reduced collisional quenching, make for better packing in the interior of the protein, improved conversion of the tyrosine to dehydrotyrosine, etc. To confirm this, further experiments need to be carried out.

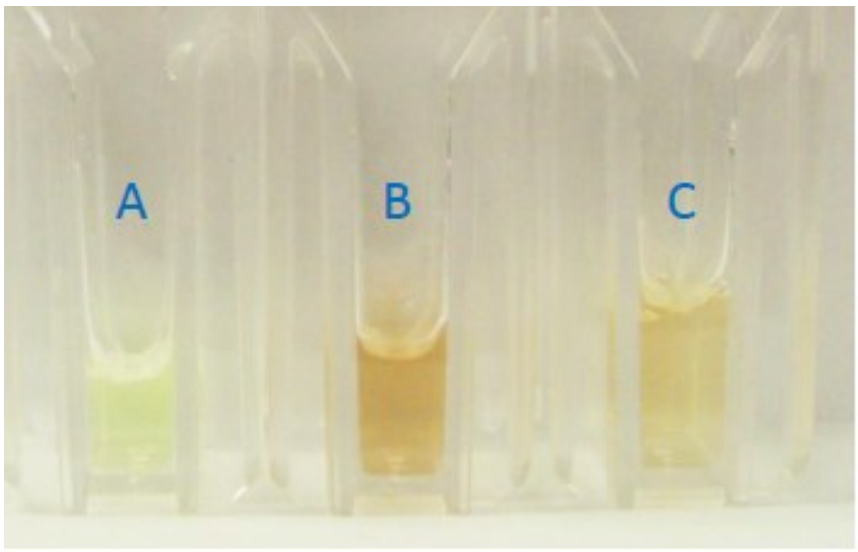

Figure 4-6: The EGFP with nine unnatural amino acids. (A) Wild-type EGFP without unnatural amino acids; (B) EGFP with nine DOPA amino acids; (C) EGFP with nine 3-NH_2Tyr amino acids.

4.4 Conclusion

We have successfully expressed and purified WT EGFP, Tyr* 9-DOPA EFGP and Tyr* 9- 3NH_2Tyr EFGP. We have shown that in the presence of UAAs in the mutants. They can be immobilized on the surface via the Diels-Alder reaction in water or the Michael addition reaction. This suggests that our strategy has the potential to immobilize bulky complex onto the surface or bioconjugate to make hydrid version with new color chromophores that may reveal valuable information about protein-protein, protein-ligand and protein-antibody interactions and to produce functional protein arrays with wilder applications in drug discovery. In addition, our mutants can be used to help further study the mechanism of EGFP fluorescence. Apparently, local protein environment in the presence of DOPA and 3-NH_2Tyr changes its color from green color (wild-type EGFP) to a brown to reddish color. In conclusion, we have generated new version of EGFP with different chemical and physical properties with these modifications.

Chapter 5

Bioconjugated Dimerization of H48(*para*-iodophenylalanine) and H48(*para*-boronophenylalanine) Myoglobin Mutants Using Suzuki Cross-Coupling Reaction

All the experiments in this chapter were done by Yanbo Zhang in the laboratory of Prof. Roshan Perera.

5.1 Introduction

If can be done, the Palladium (Pd)-catalyzed cross-coupling reaction, the Suzuki/Miyaura coupling reaction, between aryl boron and aryl halides amino acid derivatives to generate covalent carbon-carbon bond will be considered as one of the powerful new tools in bioconjugation of proteins.[87-90] Such covalently dimerized proteins can provide a platform for a catalytically enhanced (super) enzyme for catalysis due to the fact that doubling of the active sites as well as providing new protein scaffold architecture for new catalytic reactions.[91-92] Furthermore, this method can be expanded to the protein attachment to a surface as arrays which will be highly useful in protein or oligonucleotide microarrays techniques.[93-94] Furthermore, it may provide a method for the development of new imaging techniques in the field of life sciences, such as mapping the protein-protein interaction of the *in vivo* imaging experiments based on a GFP (green fluorescence protein) coupled to a target-binding protein. The Suzuki cross coupling reaction has also been previously done to couple an iodinated bodipy reporter molecule and a protein containing the unnatural amino acid *p*-boronophenylalanine.[95-97]

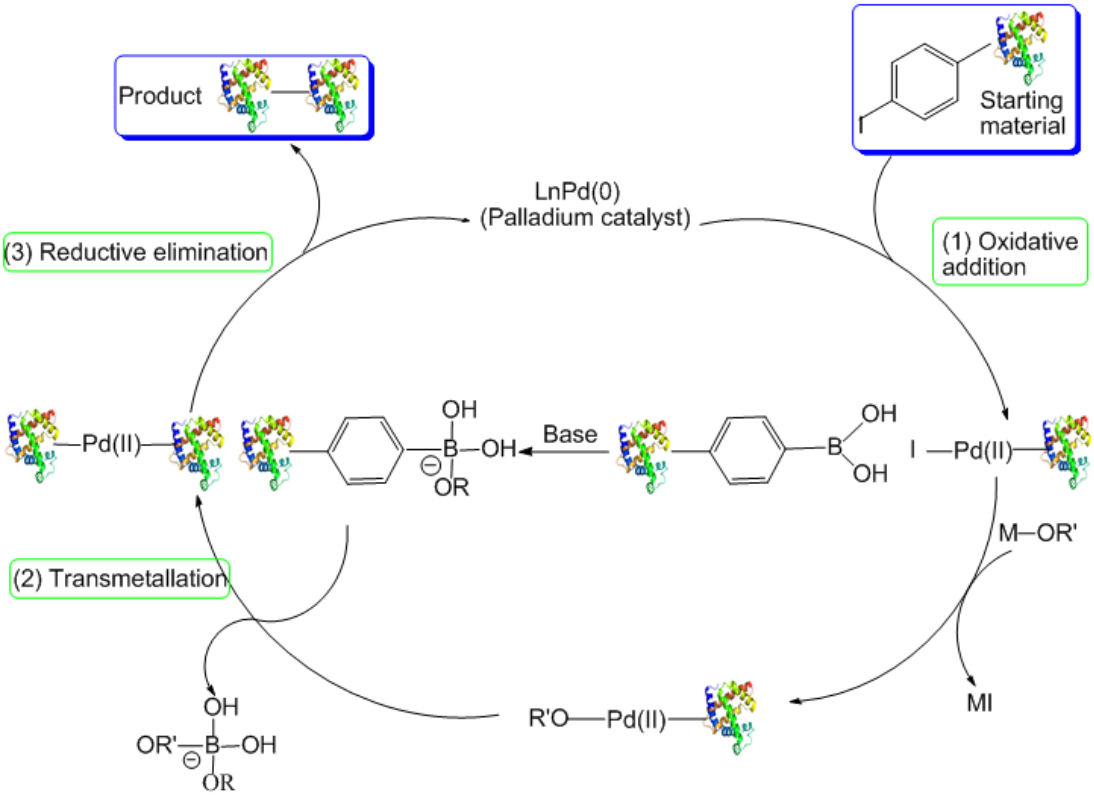

Figure 5-1: Mechanism of the Pd-catalyzed cross-coupling reaction.[98-99]

However, a monomeric protein, such as Mb is made up with 20 natural amino acids limits the introduction of such a dimerization process without a chemical modification to its existing residues or site-directly mutated residue. Recently, a new technology has been developed via unnatural amino acid introduction into proteins, at sites specifically labeled using a TAG codon (amber nonsense codon) in the gene construct, in genetic level. Site-specific incorporation of unnatural amino acids into proteins using an orthogonal tyrosyl tRNA/aminoacyl-tRNA synthetase pair from *Methanococcus jannaschii* (*Mj*) can be evolved to recognize the H48 TAG codon in the

gene. With this method, the triplet codon TAG is recognized by the unnatural amino acid charged tRNA will facilitate the incorporation of the unnatural amino acid into the protein *in vivo*.

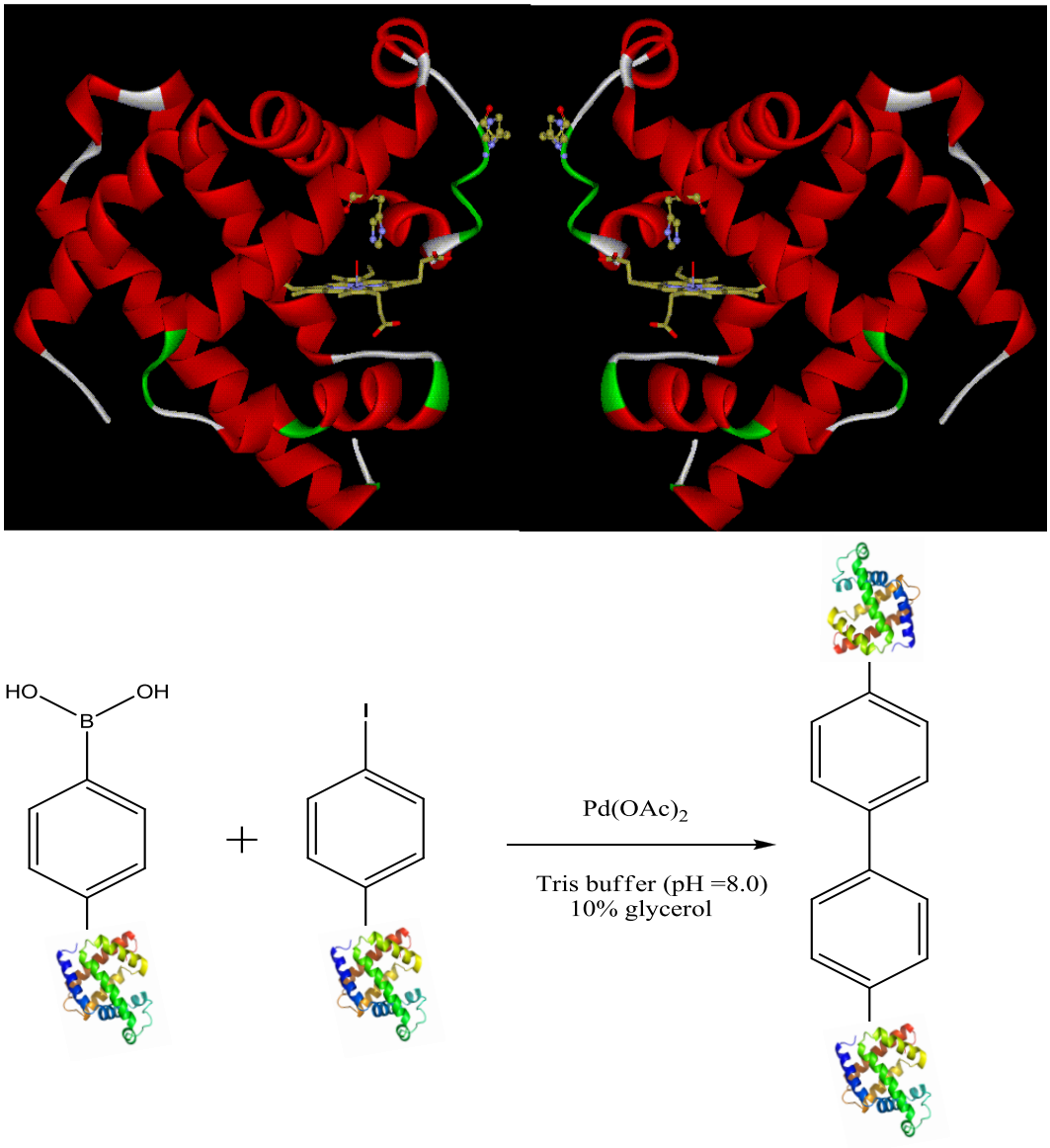

Figure 5-2: H48 labelled Mb picture to show the coupling location. The Suzuki reaction cross-coupling reaction (below)

The genetically incorporated *p*-boronophenylalanine at H48 position of Mb can easily be reacted with another genetically altered H48(*p*-iodophenyalanine) containing Mb mutant using the Suzuki coupling reaction. The main feature of a mild method to incorporate functional groups into proteins should be to preserve the native conformation (active enzyme) and prevent the denaturation during the follow up chemical coupling using Pd catalyst. The choice of the Pd complex select for the Suzuki cross-coupling reaction of proteins should primarily rely on the water solubility. There are several such complexes readily available for this reaction, such as $PdCl_2$, Na_2PdCl_4, and $Pd(OAc)_2$.[100] In our experiment, we have used $Pd(OAC)_2$ for the coupling of monomeric Mb into a dimer using the Suzuki coupling reaction. Herein we are reporting successfully coupled Mb containing a boronic acid to a *para*-iodophenylalanine with Mb using a water soluble palladium catalyst, $Pd(OAC)_2$.

5.2 Materials and Methods

5.2.1 *Expression of H48(p-Iodophenylalanine) Mb*

30 µL of DH10B *E. coli* competence cells (were pipetted into an electroporation cuvette) were cotransformed with H48TAG Mb gene containing pBAD plasmid (with kanamycin resistance marker) and pSUP tRNA/aminoacyl-tRNA synthetase pair (which is evolved for the *p*-boronophenylalanine or *p*-iodophenylalanine) plasmid with chloramphenicol resistance marker using electroporation. Recovery of the cells were done by mixing with 200 µL of S.O.C media (one mL of S.O.C mixed with 20 µL of 18% glycerol) and pipetted into a plastic vial. The solution was incubated at 37 °C for 1h. After 1h, the cells were streaked onto an agar plate containing kanamycin and

chloramphenicol (final concentration 25 μg/mL each). The plate was allowed to incubate at 37 °C for one day. One colony of cells was retrieved from the agar plate and incubated overnight at 37 °C in a solution of 20 mL of LB medium (with kanamycin and chloramphenicol antibiotics). The 20 mL solution was then incubated in 1 L of LB medium (with the same antibiotics). When the optical density of the solution at OD_{600} nm reached 0.5, *p*-boronophenylalanine or *p*-iodophenylalanine amino acid was added. The cells were allowed to grow until the optical density at 600 nm reached 0.5, at which they were induced with Isopropyl β-D-1-thiogalactopyranoside. The temperature of the incubator was then adjusted to 30 °C, and the cells incubated for about 10h (overnight). After incubation, the culture was moved into a 4°C refrigerator.

A starter culture was made by inoculating 20 mL of LB medium containing kanamycin and chloramphenicol (final concentration of 100 μg/mL and 33.3 μg/mL, respectively) with cell stocks that contained the pBAD plasmid with H48 TAG Mb gene and pSUP plasmid with *p-iodophenylalanine* tRNA/aminoacyl-tRNA synthetase pair. The culture was incubated at 37 °C overnight. A 1 L culture was inoculated with the starter culture and grown at 37 °C until the OD_{600} reached 0.5. At this point the culture was charged with the unnatural amino acid *para*-iodophenylalanine or *p*-boronophenylalanine to a final concentration of 1 mM. The cells were then allowed to grow until the OD_{600} reached 0.5, at which point it was induced with 10 mL of 20% arabinose. The culture was then grown for about 10h at 30 °C. After growth, the culture was moved into a 4 °C refrigerator until the protein was to be purified.

5.2.2 *Purification of H48 (p-iodophenylalanine) Mb and H48(p-boronophenylalanine) Mb Mutants*

The following procedure was used to purify both mutant proteins. The 1 L LB medium was centrifuged at 10000 rpm, 4 °C, for 10 min. The cell pellet was suspended and dissolved in Tris HCl (pH 8.0). RNase, DNase, and lysozyme were added to the resulting solution. The solution was then shaken slowly for 45 min on ice. The solution was flash frozen in liquid nitrogen, and thawed out in a water bath at 37 °C. The freezing and thawing was repeated two more times. The solution was sonicated for 2 min for 30 seconds intervals. The resulting solution was then centrifuged at 10000 rpm, 4 °C, for 10 min. The supernatant was poured into a clean vial and 3 mL of Ni-NTA Resin was added to it. The slurry was centrifuged at 1000 rpm, 4 °C, for one minute. To recover the pure protein the Mb mutants, the supernatant was poured out and discarded, and the protein was applied to a column, then wash with Tris buffer at pH 8.0 (with 10 mM imidazole), and finally elute with elute buffer, Tris buffer at pH 8.0, (with 250 mM imidazole). The purified protein (red in color) was collected in fractions.

5.2.3 *Set Up of Reaction and Collection of Data*

The Suzuki cross coupling reaction between H48 *p*-boronohenylalanine Mb and H48 *p*-iodophenylalanine Mb was done in 50 mM Tris HCl buffer at pH 8.0 with 10% glycerol. To a solution of 10 μM H48 *p*-iodophenylalanine Mb reaction mixture, 2 mM of $Pd(OAc)_2$ was added in Tris HCl buffer. Then 10 μM of H48(*p*-boronophenylalanine) Mb was added and pipetted up and down to mix. The tube was then put on a heating block at 40°C for 18h. After 18h, the solution was dialyzed in dialysis buffer (200 mM Tris HCl buffer at pH 5.0, 1 mM EDTA, and 10% glycerol) at 4 °C to remove the excess Pd. The dialyzed solution was run on a SDS-PAGE protein gel and analysis on MALDI for the product confirmation.

5.3 Results and Discussion

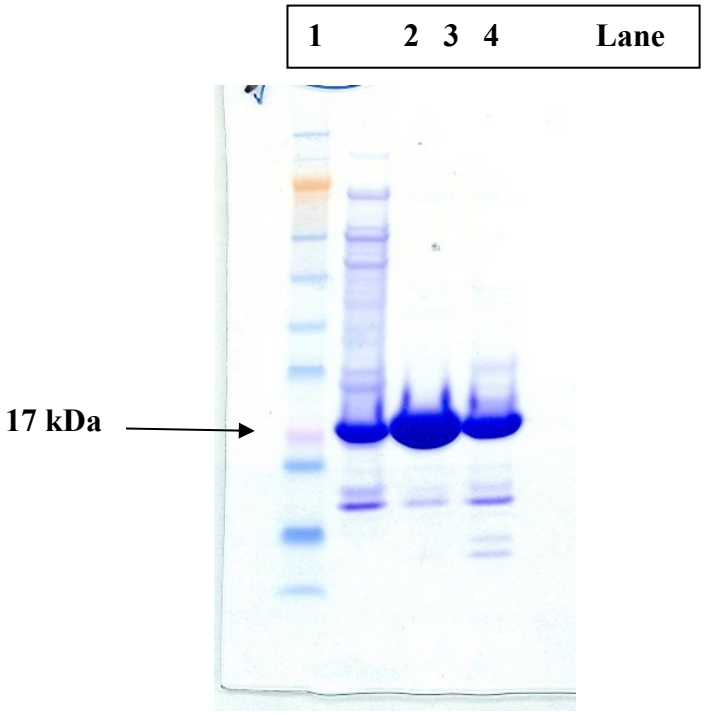

Figure 5-3: The SDS-PAGE gel of Mb after purification using Ni-NTA. Lane 1: protein ladder; Lane 2: monomeric wild-type Mb; Lane 3: H48(*p*-boronophenylalanine) mutant Mb and Lane 4: H48(*p*-iodophenylalanine) mutant Mb

Figure 5-3 shows the SDS-PAGE gel for the expression and purification of wild-type and two mutants of Mb. Based on the gel it can be concluded that in fact H48(p-boronophenylalanine) mutant Mb over expresses much more than the H48(*p*-iodophenylalanine) mutant Mb under the same condition. The Ni-NTA purified protein seems to be very high (90%) or above for the two mutants. These proteins were directly used in the cross-coupling reaction with $Pd(OAc)_2$ after buffer exchanged in Tris HCl buffer at pH 8.0.

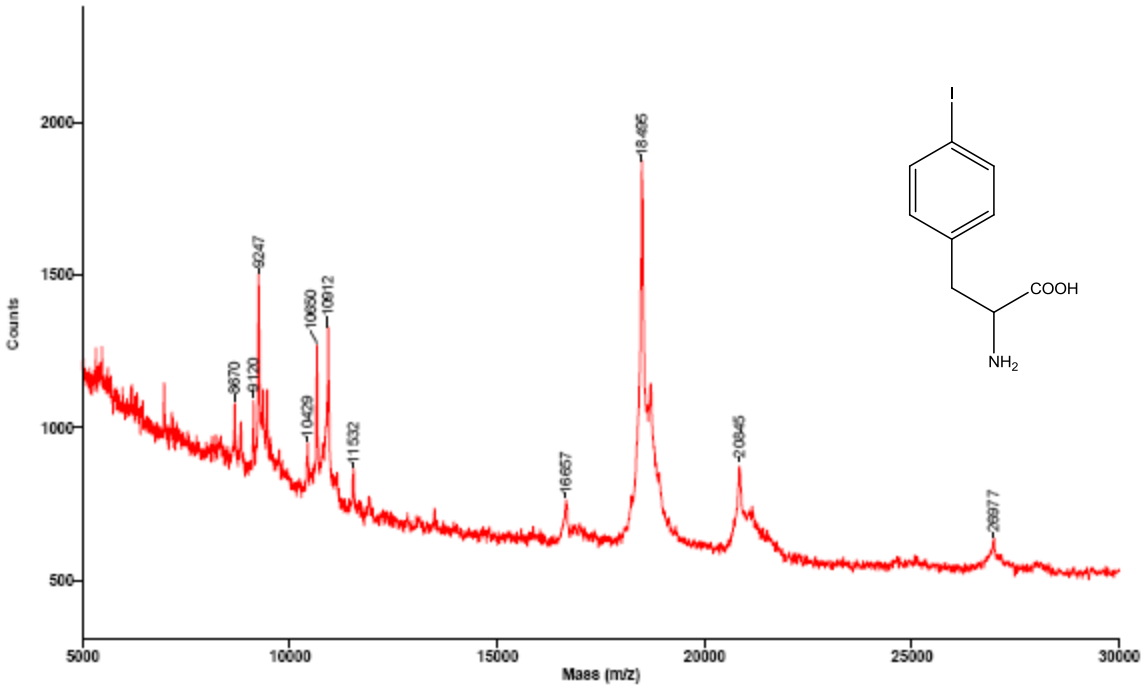

Figure 5-4: The MS spectrum (MALDI) of the H48(*para*-Iodophenylalanine) mutant Mb. The expected mass (with the Met residue) is 18,492 and observed mass is 18,495.

The MALDI mass spectrum of the H48(*para*-Iodophenylalanine) mutant Mb in Figure 5-4 shows that the mass of the mutant Mb (18,495 a.m.u.) has a close match to the expected mass (18,492 a.m.u.) within margin of error of the instrument. Competitive incorporation of tyrosine (back ground expression based on *mj* tyrosyl synthetase) should show at 18,381 a.m.u and also wild-type of Mb is expected to appear at 18,335. Absence of these peaks suggests that the *para*-Iodophenylalanine has been successfully incorporated at the position H48 in Mb.

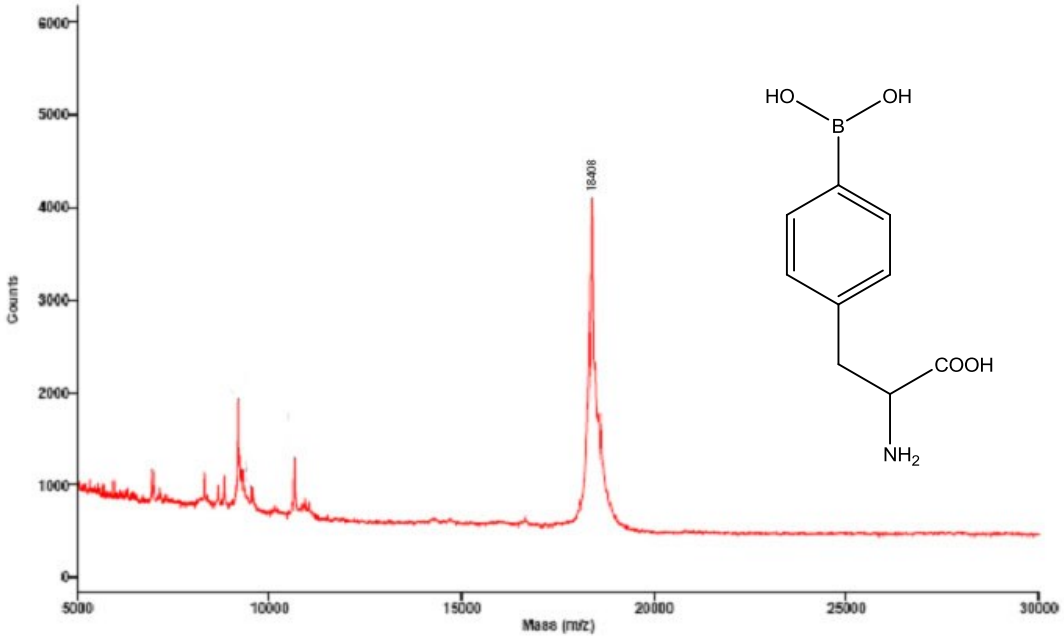

Figure 5-5: The MS spectrum (MALDI) of the H48(*para*-boronohenylalanine) mutant Mb. The expected mass (with the Met residue is 18,410) closely matches with the observed mass of 18,408 a.m.u.

In Figure 5-5, the H48(*para*-boronohenylalanine) mutant Mb shows the expected mass of 18,410 in the MALDI spectrum suggesting that intact protein had been expressed in *E. Coli*. In the absence of 18,381 a.m.u peak in the spectrum, it can be concluded that there is no synthetase competitive Tyr incorporation in protein at H48 position. WT Mb peak is also clearly absent in this work.

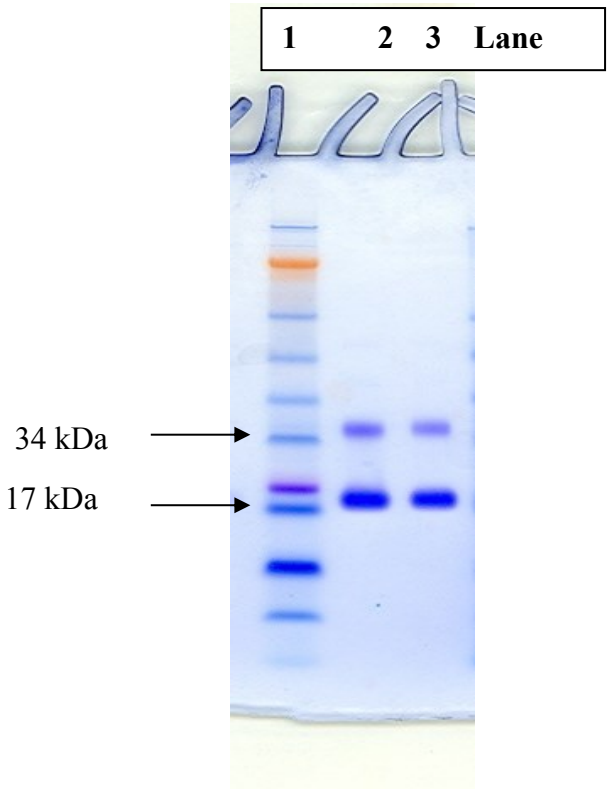

Figure 5-6: The SDS-PAGE gel for the coupling-reaction between the H48(*para*-boronophenylalanine) mutant Mb and the H48(*para*-iodophenylalanine) mutant Mb (25 μM of each protein) carried out using $Pd(OAc)_2$ catalyst at RT for 4h in 50 mM Tris buffer with 10% glycerol at pH 8.0. Lane 1 is the protein ladder. Lane 2 has the catalyst concentration of 4 mM and Lane 3 has 2 mM, respectively.

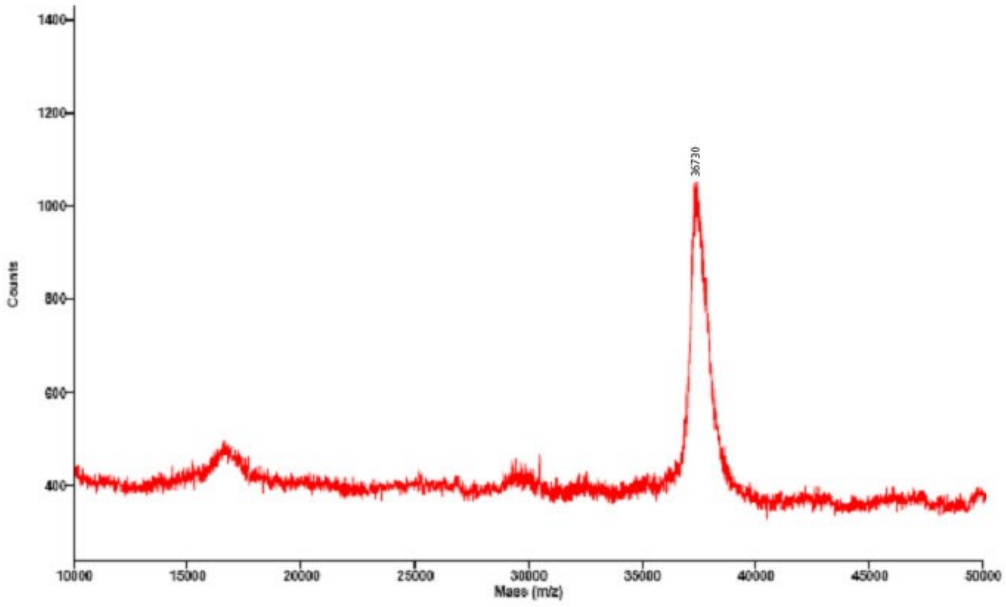

Figure 5-7: The MALDI spectrum of the dimer product. The peak is appeared ta the expected mass of 36,730 a.m.u.

From the protein gel, Figure 5-6, it is clear that the Suzuki coupling reaction was successful. The product of the coupling (lane 2), does appear to have dimer bands on the gel. Furthermore, by examining the peak at 37 kDa, MALDI spectrum of the reaction mixture (after dialysis in the buffer) suggests that 15-20% or so dimer formation. If increase the $Pd(OAc)_2$ catalyst concentration from 2 mM to 4mM, there seems to be more dimer formation as shown SDS-PAGE gel in Figure 5-6.

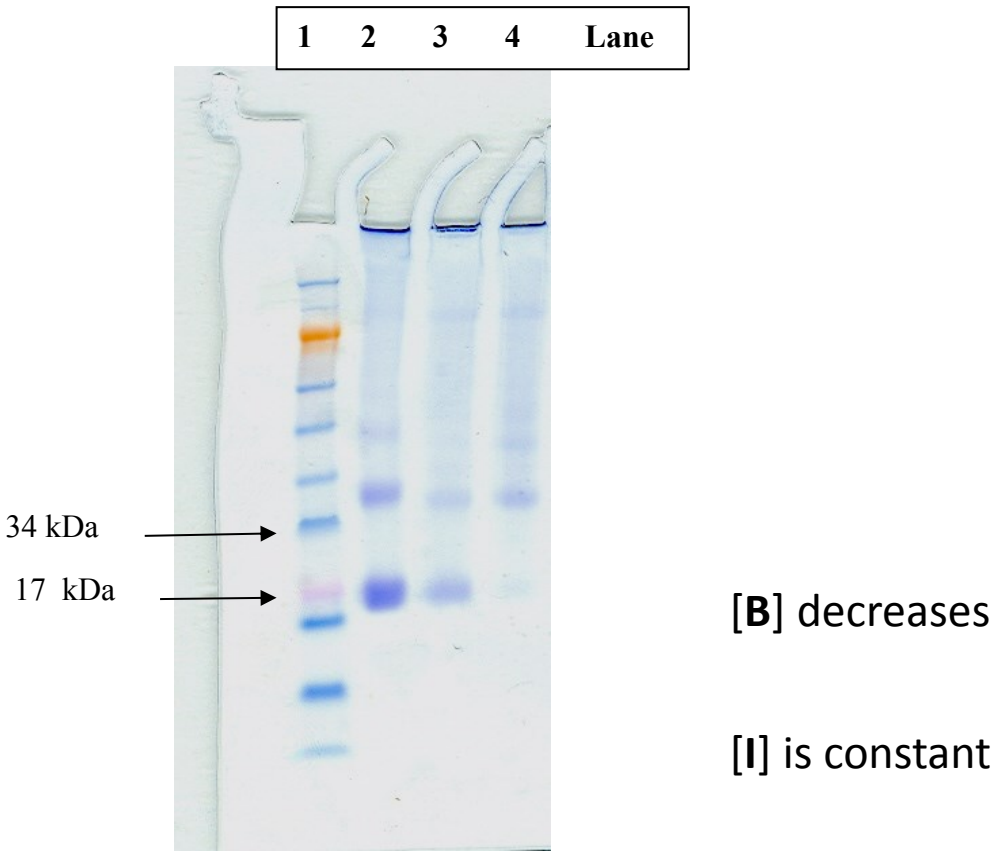

Figure 5-8: The SDS-PAGE gel for the overnight coupling-reaction between the H48(*para*-boronophenylalanine) mutant Mb and the H48(*para*-iodophenylalanine) mutant Mb carried out using $Pd(OAc)_2$ as the catalyst (2 mM) at RT in 50 mM Tris buffer with 10% glycerol at pH 8.0. Lane 1 is the protein ladder. This gel was done with a changing concentration of the H48(*para*-boronophenylalanine) mutant Mb (Lane 2: 15 μM; Lane 3: 10 μM and Lane 4: 5 μM) with the constant H48(*para*-iodophenylalanine) mutant Mb (5 μM) and catalyst concentrations (2 mM).

Based on Figure 5-6 experiment, it is clear that if H48(*para*-iodophenylalanine) mutant Mb kept constant at 5 μM while the concentration of H48(*para*-boronophenylalanine) mutant Mb decreases from 15 μM, 10 μM, and 5 μM, coupling reaction can be optimized with 2 mM catalyst at room temperature.

5.4 Conclusion

It can be concluded from the presented data that in Suzuki cross-coupling reaction between two mutants Mbs [H48(*para*-iodophenylalanine) and H48(*para*-boronophenylalanine)] was a success with the $Pd(OAc)_2$ catalyst. However, in order to achieve the complete coupling reaction, there should be longer than 4h coupling (for example, overnight or longer coupling time). This bioconjugate Suzuki cross-coupling reaction can be expanded with other proteins as well, making it a versatile method for protein tagging to surface, to *in vivo* image experiment.

References

(1) Lindgren, H.; Shen, H.; Zingmark, C.; Golovliov, I.; Conlan, W.; Sjostedt, A., "Resistance of *Francisella tularensis* strains against reactive nitrogen and oxygen species with special reference to the role of KatG", *Infect. Immun.* **2007**, *75*, 1303-9.

(2) Smulevich, G.; Jakopitsch, C.; Droghetti, E.; Obinger, C., "Probing the structure and bifunctionality of catalase-peroxidase (KatG)", *J. Inorg. Biochem.* **2006**, *100*, 568-85.

(3) Jaber, M.; Rattan, A.; Kumar, R., "Presence of katG gene in resistant *Mycobacterium tuberculosis*", *J. Clin. Pathol.* **1996**, *49*, 945-7.

(4) Shim, T. S.; Yoo, C. G.; Han, S. K.; Shim, Y. S.; Kim, Y. W., "Isoniazid resistance and the point mutation of codon 463 of katG gene of *Mycobacterium tuberculosis*", *J. Korean Med. Sci.* **1997**, *12*, 92-8.

(5) Bergval, I. L.; Schuitema, A. R.; Klatser, P. R.; Anthony, R. M., "Resistant mutants of *Mycobacterium tuberculosis* selected in vitro do not reflect the in vivo mechanism of isoniazid resistance", *J. Antimicrob. Chemother.* **2009**, *64*, 515-23.

(6) Goyal, M.; Young, D.; Zhang, Y.; Jenkins, P. A.; Shaw, R. J., "PCR amplification of variable sequence upstream of katG gene to subdivide strains of *Mycobacterium tuberculosis* complex", *J. Clin. Microbiol.* **1994**, *32*, 3070-1.

(7) Zhang, Y.; Young, D., "Strain variation in the katG region of *Mycobacterium tuberculosis*", *Mol. Microbiol.* **1994**, *14*, 301-8.

(8) Ferrazoli, L.; Palaci, M.; Telles, M. A.; Ueki, S. Y.; Kritski, A.; Marques, L. R.; Ferreira, O. C.; Riley, L. W., "Catalase expression, katG, and MIC of isoniazid for *Mycobacterium tuberculosis* isolates from Sao Paulo, Brazil", *J. Infect. Dis.* **1995**, *171*, 237-40.

(9) Pym, A. S.; Domenech, P.; Honore, N.; Song, J.; Deretic, V.; Cole, S. T., "Regulation of catalase-peroxidase (KatG) expression, isoniazid sensitivity and virulence by furA of *Mycobacterium tuberculosis*", *Mol. Microbiol.* **2001**, *40*, 879-89.

(10) Chouchane, S.; Lippai, I.; Magliozzo, R. S., "Catalase-peroxidase (*Mycobacterium tuberculosis* KatG) catalysis and isoniazid activation", *Biochemistry* **2000**, *39*, 9975-83.

(11) Ramasubban, G.; Therese, K. L.; Vetrivel, U.; Sivashanmugam, M.; Rajan, P.; Sridhar, R.; Madhavan, H. N.; Meenakshi, N., "Detection of novel coupled mutations in the katG gene (His276Met, Gln295His and Ser315Thr) in a multidrug-resistant *Mycobacterium tuberculosis* strain from Chennai, India, and insight into the molecular mechanism of isoniazid resistance using structural bioinformatics approaches", *Int. J. Antimicrob. Agents* **2011**, *37*, 368-72.

(12) Mo, L.; Zhang, W.; Wang, J.; Weng, X. H.; Chen, S.; Shao, L. Y.; Pang, M. Y.; Chen, Z. W., "Three-dimensional model and molecular mechanism of *Mycobacterium*

tuberculosis catalase-peroxidase (KatG) and isoniazid-resistant KatG mutants", *Microb. Drug Resist.* **2004**, *10*, 269-79.

(13) Vlasits, J.; Furtmuller, P. G.; Jakopitsch, C.; Zamocky, M.; Obinger, C., "Probing hydrogen peroxide oxidation kinetics of wild-type Synechocystis catalase-peroxidase (KatG) and selected variants", *Biochim. Biophys. Acta.* **2010**, *1804*, 799-805.

(14) Lee, H. I.; Yoon, J. H.; Nam, J. S.; Kim, Y. M.; Ro, Y. T., "Cloning, expression and characterization of the catalase-peroxidase (KatG) gene from a fast-growing *Mycobacterium sp. strain JC1 DSM 3803*", *J. Biochem.* **2010**, *147*, 511-22.

(15) Johnsson, K.; Froland, W. A.; Schultz, P. G., "Overexpression, purification, and characterization of the catalase-peroxidase KatG from *Mycobacterium tuberculosis*", *J. Biol. Chem.* **1997**, *272*, 2834-40.

(16) Ten, I. T.; Kumasaka, T.; Higuchi, W.; Tanaka, S.; Yoshimatsu, K.; Fujiwara, T.; Sato, T., "Expression, purification, crystallization and preliminary X-ray analysis of the Met244Ala variant of catalase-peroxidase (KatG) from the *haloarchaeon Haloarcula marismortui*", *Acta. Crystallogr. Sect. F. Struct. Biol. Cryst. Commun.* **2007**, *63*, 940-3.

(17) Carpena, X.; Loprasert, S.; Mongkolsuk, S.; Switala, J.; Loewen, P. C.; Fita, I., "Catalase-peroxidase KatG of *Burkholderia pseudomallei* at 1.7A resolution", *J. Mol. Biol.* **2003**, *327*, 475-89.

(18) Wang, Y.; Goodwin, D. C., "Integral role of the I'-helix in the function of the "inactive" C-terminal domain of catalase-peroxidase (KatG)", *Biochim. Biophys. Acta.* **2013**, *1834*, 362-71.

(19) Wang, L.; Brock, A.; Herberich, B.; Schultz, P. G., "Expanding the genetic code of *Escherichia coli*", *Science* **2001**, *292*, 498-500.

(20) Magliery, T. J.; Anderson, J. C.; Schultz, P. G., "Expanding the genetic code: selection of efficient suppressors of four-base codons and identification of "shifty" four-base codons with a library approach in *Escherichia coli*", *J. Mol. Biol.* **2001**, *307*, 755-69.

(21) Wang, L.; Xie, J.; Schultz, P. G., "Expanding the genetic code", *Annu. Rev. Biophys. Biomol. Struct.* **2006**, *35*, 225-49.

(22) Schultz, K. C.; Supekova, L.; Ryu, Y.; Xie, J.; Perera, R.; Schultz, P. G., "A genetically encoded infrared probe", *J. Am. Chem. Soc.* **2006**, *128*, 13984-5.

(23) Mehl, R. A.; Anderson, J. C.; Santoro, S. W.; Wang, L.; Martin, A. B.; King, D. S.; Horn, D. M.; Schultz, P. G., "Generation of a bacterium with a 21 amino acid genetic code", *J. Am. Chem. Soc.* **2003**, *125*, 935-9.

(24) Xie, J.; Schultz, P. G., "Adding amino acids to the genetic repertoire", *Curr. Opin. Chem. Biol.* **2005**, *9*, 548-54.

(25) Alfonta, L.; Zhang, Z.; Uryu, S.; Loo, J. A.; Schultz, P. G., "Site-specific incorporation of a redox-active amino acid into proteins", *J. Am. Chem. Soc.* **2003**, *125*, 14662-3.

(26) Jiang, M.; Wang, K.; Kennedy, J. F.; Nie, J.; Yu, Q.; Ma, G., "Preparation and characterization of water-soluble chitosan derivative by Michael addition reaction", *Int. J. Biol. Macromol.* **2010**, *47*, 696-9.

(27) Ng, V. H.; Cox, J. S.; Sousa, A. O.; MacMicking, J. D.; McKinney, J. D., "Role of KatG catalase-peroxidase in mycobacterial pathogenesis: countering the phagocyte oxidative burst", *Mol. Microbiol.* **2004**, *52*, 1291-302.

(28) Goth, L., "Reactive oxygen species, hydrogen peroxide, catalase and diabetes mellitus", *Redox Rep.* **2006**, *11*, 281-2.

(29) Vlasits, J.; Jakopitsch, C.; Schwanninger, M.; Holubar, P.; Obinger, C., "Hydrogen peroxide oxidation by catalase-peroxidase follows a non-scrambling mechanism", *FEBS Lett.* **2007**, *581*, 320-4.

(30) Chance, B.; Oshino, N., "Analysis of the catalase--hydrogen peroxide intermediate in coupled oxidations", *Biochem. J.* **1973**, *131*, 564-7.

(31) Wiesner, K., "The reaction mechanism of catalase", *Experientia* **1962**, *18*, 115-6.

(32) Rodionova, I. V., "Peroxidase activity of tularemia bacteria", *Zh. Mikrobiol. Epidemiol. Immunobiol.* **1981**, 101-2.

(33) Ivancich, A.; Donald, L. J.; Villanueva, J.; Wiseman, B.; Fita, I.; Loewen, P. C., "Spectroscopic and Kinetic Investigation of the Reactions of Peroxyacetic Acid with Burkholderia pseudomallei Catalase-Peroxidase, KatG", *Biochemistry* **2013**, *52*, 7271-82.

(34) Nagano, S.; Yamashita, T.; Mimura, K.; Matsuoka, A., "[Peroxidase stain of leucocytes with combination of alpha-naphthol and anilin dyes (author's transl)]", *Rinsho. Byori.* **1979**, *27*, 70-2.

(35) Xu, F.; Koch, D. E.; Kong, I. C.; Hunter, R. P.; Bhandari, A., "Peroxidase-mediated oxidative coupling of 1-naphthol: characterization of polymerization products", *Water Res.* **2005**, *39*, 2358-68.

(36) Wang, R. F.; Wennerstrom, D.; Cao, W. W.; Khan, A. A.; Cerniglia, C. E., "Cloning, expression, and characterization of the katG gene, encoding catalase-peroxidase, from the polycyclic aromatic hydrocarbon-degrading bacterium *Mycobacterium sp. strain PYR-1*", *Appl. Environ. Microbiol.* **2000**, *66*, 4300-4.

(37) Bhandari, A.; Xu, F.; Koch, D. E.; Hunter, R. P., "Peroxidase-mediated polymerization of 1-naphthol: impact of solution pH and ionic strength", *J. Environ. Qual.* **2009**, *38*, 2034-40.

(38) Beier, M.; Hoheisel, J. D., "Versatile derivatisation of solid support media for covalent bonding on DNA-microchips", *Nucleic Acids Res.* **1999**, *27*, 1970-7.

(39) Flachsbart, H.; Stober, W., "Preparation of radioactively labeled monodisperse silica spheres of colloidal size", *J. Colloid Interface Sci.* **1969**, *30*, 568-73.

(40) Gentili, D.; Ori, G.; Comes Franchini, M., "Double phase transfer of gold nanorods for surface functionalization and entrapment into PEG-based nanocarriers", *Chem. Commun. (Camb)* **2009**, 5874-6.

(41) Heggli, M.; Tirelli, N.; Zisch, A.; Hubbell, J. A., "Michael-type addition as a tool for surface functionalization", *Bioconjug. Chem.* **2003**, *14*, 967-73.

(42) Mansur, H. S.; Lobato, Z. P.; Orefice, R. L.; Vasconcelos, W. L.; Oliveira, C.; Machado, L. J., "Surface functionalization of porous glass networks: effects on bovine serum albumin and porcine insulin immobilization", *Biomacromolecules* **2000**, *1*, 789-97.

(43) Adhikari, P. D.; Tai, Y.; Ujihara, M.; Chu, C. C.; Imae, T.; Motojima, S., "Surface functionalization of carbon micro coils and their selective immobilization on surface-modified silicon substrates", *J. Nanosci. Nanotechnol* **2010**, *10*, 833-9.

(44) Verheyen, E.; Delain-Bioton, L.; der Wal, S.; El Morabit, N.; Hennink, W. E.; van Nostrum, C. F., "Protein macromonomers for covalent immobilization and subsequent triggered release from hydrogels", *J. Control Release* **2010**, *148*, e18-9.

(45) Schillemans, J. P.; Hennink, W. E.; van Nostrum, C. F., "The effect of network charge on the immobilization and release of proteins from chemically crosslinked dextran hydrogels", *Eur. J. Pharm. Biopharm.* **2010**, *76*, 329-35.

(46) Choi, D.; Lee, W.; Park, J.; Koh, W., "Preparation of poly(ethylene glycol) hydrogels with different network structures for the application of enzyme immobilization", *Biomed. Mater. Eng.* **2008**, *18*, 345-56.

(47) Iso, M.; Shirahase, T.; Hanamura, S.; Urushiyama, S.; Omi, S., "Immobilization of enzyme by microencapsulation and application of the encapsulated enzyme in the catalysis", *J. Microencapsul.* **1989**, *6*, 165-76.

(48) Maeda, Y.; Yoshino, T.; Takahashi, M.; Ginya, H.; Asahina, J.; Tajima, H.; Matsunaga, T., "Noncovalent immobilization of streptavidin on in vitro- and in vivo-biotinylated bacterial magnetic particles", *Appl. Environ. Microbiol.* **2008**, *74*, 5139-45.

(49) Sadurni, P.; Alagon, A.; Aliev, R.; Burillo, G.; Hoffman, A. S., "Immobilization of streptavidin-horseradish peroxidase onto a biotinylated poly(acrylic acid) backbone that had been radiation-grafted to a PTFE film", *J. Biomater. Sci. Polym. Ed.* **2005**, *16*, 181-7.

(50) Kossek, S.; Padeste, C.; Tiefenauer, L., "Immobilization of streptavidin for immunosensors on nanostructured surfaces", *J. Mol. Recognit.* **1996**, *9*, 485-7.

(51) Kumar, S. A.; Chen, S. M., "Direct electrochemistry and electrocatalysis of myoglobin on redox-active self-assembling monolayers derived from nitroaniline modified electrode", *Biosens. Bioelectron.* **2007**, *22*, 3042-50.

(52) Yi, X.; Huang-Xian, J.; Hong-Yuan, C., "Direct electrochemistry of horseradish peroxidase immobilized on a colloid/cysteamine-modified gold electrode", *Anal. Biochem.* **2000**, *278*, 22-8.

(53) Kong, Y. T.; Boopathi, M.; Shim, Y. B., "Direct electrochemistry of horseradish peroxidase bonded on a conducting polymer modified glassy carbon electrode", *Biosens. Bioelectron* **2003**, *19*, 227-32.

(54) d'Arcy Doherty, M.; Wilson, I.; Wardman, P.; Basra, J.; Patterson, L. H.; Cohen, G. M., "Peroxidase activation of 1-naphthol to naphthoxy or naphthoxy-derived radicals and their reaction with glutathione", *Chem. Biol. Interact.* **1986**, *58*, 199-215.

(55) von Woedtke, T.; Fischer, U.; Abel, P., "Glucose oxidase electrodes: effect of hydrogen peroxide on enzyme activity?", *Biosens. Bioelectron.* **1994**, *9*, 65-71.

(56) Collins, L. Z.; Maggio, B.; Gallagher, A.; York, M.; Schafer, F., "Safety evaluation of a novel whitening gel, containing 6% hydrogen peroxide and a commercially available whitening gel containing 18% carbamide peroxide in an exaggerated use clinical study", *J. Dent.* **2004**, *32 Suppl 1*, 47-50.

(57) Hiti, K.; Walochnik, J.; Haller-Schober, E. M.; Faschinger, C.; Aspock, H., "Viability of Acanthamoeba after exposure to a multipurpose disinfecting contact lens solution and two hydrogen peroxide systems", *Br. J. Ophthalmol.* **2002**, *86*, 144-6.

(58) Bruce, A. S., "Hydration of hydrogel contact lenses during hydrogen peroxide disinfection", *J. Am. Optom. Assoc.* **1989**, *60*, 581-2.

(59) Harris, M. G., "Practical considerations in the use of hydrogen peroxide disinfection systems", *CLAO J.* **1990**, *16*, S53-60.

(60) Kaplan, E. N.; Gundel, R. E.; Sosale, A.; Sack, R., "Residual hydrogen peroxide as a function of platinum disc age", *CLAO J.* **1992**, *18*, 149-54.

(61) Hillar, A.; Nicholls, P., "A mechanism for NADPH inhibition of catalase compound II formation", *FEBS Lett.* **1992**, *314*, 179-82.

(62) Kirkman, H. N.; Galiano, S.; Gaetani, G. F., "The function of catalase-bound NADPH", *J. Biol. Chem.* **1987**, *262*, 660-6.

(63) Harris, M. G.; Torres, J.; Tracewell, L., "pH and H2O2 concentration of hydrogen peroxide disinfection systems", *Am. J. Optom. Physiol. Opt.* **1988**, *65*, 527-35.

(64) Harris, M. G.; Gan, C. M.; Long, D. A.; Cushing, L. A., "The pH of over-the-counter hydrogen peroxide in soft lens disinfection systems", *Optom. Vis. Sci.* **1989**, *66*, 839-42.

(65) Zhou, L.; Elias, R. J., "Investigating the hydrogen peroxide quenching capacity of proteins in polyphenol-rich foods", *J. Agric. Food Chem.* **2011**, *59*, 8915-22.

(66) Spreti, N.; Bartoletti, A.; Di Profio, P.; Germani, R.; Savelli, G., "Effects of ionic and zwitterionic surfactants on the stabilization of bovine catalase", *Biotechnol. Prog.* **1995**, *11*, 107-11.

(67) Blanco, E.; Ruso, J. M.; Prieto, G.; Sarmiento, F., "Different thermal unfolding pathways of catalase in the presence of cationic surfactants", *J. Phys. Chem. B.* **2007**, *111*, 2113-8.

(68) Dani, C.; Buonocore, G.; Longini, M.; Felici, C.; Rodriguez, A.; Corsini, I.; Rubaltelli, F. F., "Superoxide dismutase and catalase activity in naturally derived commercial surfactants", *Pediatr. Pulmonol.* **2009**, *44*, 1125-31.

(69) Huckaba, C. E.; Keyes, F. G., "The accuracy of estimation of hydrogen peroxide by potassium permanganate titration", *J. Am. Chem. Soc.* **1948**, *70*, 1640-4.

(70) Xu, X. X.; Zhang, J. X.; Guo, F.; Zheng, W.; Zhou, H. M.; Wang, B. L.; Zheng, Y. F.; Wang, Y. B.; Cheng, Y.; Lou, X.; Jang, B. Z., "A novel amperometric hydrogen peroxide biosensor based on immobilized Hb in Pluronic P123-nanographene platelets composite", *Colloids Surf. B. Biointerfaces* **2011**, *84*, 427-32.

(71) Dabrowska, M.; Hendrikx, P. J.; Skierski, J.; Malinowska, M.; Bertino, J. R.; Rode, W., "EGFP fluorescence as an indicator of cancer cells response to methotrexate", *Eur. J. Pharmacol.* **2007**, *555*, 93-9.

(72) Giel-Moloney, M.; Krause, D. S.; Chen, G.; Van Etten, R. A.; Leiter, A. B., "Ubiquitous and uniform in vivo fluorescence in ROSA26-EGFP BAC transgenic mice", *Genesis* **2007**, *45*, 83-9.

(73) Gohar, A. V.; Cao, R.; Jenkins, P.; Li, W.; Houston, J. P.; Houston, K. D., "Subcellular localization-dependent changes in EGFP fluorescence lifetime measured by time-resolved flow cytometry", *Biomed. Opt. Express* **2013**, *4*, 1390-400.

(74) Ding, F.; Lee, K. J.; Vahedi-Faridi, A.; Huang, T.; Xu, X. H., "Design and probing of efflux functions of EGFP fused ABC membrane transporters in live cells using fluorescence spectroscopy", *Anal. Bioanal. Chem.* **2011**, *400*, 223-35.

(75) Follenius-Wund, A.; Bourotte, M.; Schmitt, M.; Iyice, F.; Lami, H.; Bourguignon, J. J.; Haiech, J.; Pigault, C., "Fluorescent derivatives of the GFP chromophore give a new insight into the GFP fluorescence process", *Biophys. J.* **2003**, *85*, 1839-50.

(76) Amoh, Y.; Bouvet, M.; Li, L.; Tsuji, K.; Moossa, A. R.; Katsuoka, K.; Hoffman, R. M., "Visualization of nascent tumor angiogenesis in lung and liver metastasis by differential dual-color fluorescence imaging in nestin-linked-GFP mice", *Clin. Exp. Metastasis* **2006**, *23*, 315-22.

(77) Mochizuki, Y.; Nakanishi, H.; Kodera, Y.; Ito, S.; Yamamura, Y.; Kato, T.; Hibi, K.; Akiyama, S.; Nakao, A.; Tatematsu, M., "TNF-alpha promotes progression of peritoneal metastasis as demonstrated using a green fluorescence protein (GFP)-tagged human gastric cancer cell line", *Clin. Exp. Metastasis* **2004**, *21*, 39-47.

(78) Aubert, J.; Stavridis, M. P.; Tweedie, S.; O'Reilly, M.; Vierlinger, K.; Li, M.; Ghazal, P.; Pratt, T.; Mason, J. O.; Roy, D.; Smith, A., "Screening for mammalian neural genes via fluorescence-activated cell sorter purification of neural precursors from Sox1-gfp knock-in mice", *Proc. Natl Acad. Sci. U S A* **2003**, *100 Suppl 1*, 11836-41.

(79) Lewis, J. C.; Daunert, S., "Dual detection of peptides in a fluorescence binding assay by employing genetically fused GFP and BFP mutants", *Anal. Chem.* **1999**, *71*, 4321-7.

(80) Youvan, D. C.; Michel-Beyerle, M. E., "Structure and fluorescence mechanism of GFP", *Nat. Biotechnol.* **1996**, *14*, 1219-20.

(81) Stamos, B.; Loredo, L.; Chand, S.; Phan, T. V.; Zhang, Y.; Mohapatra, S.; Rajeshwar, K.; Perera, R., "Biosynthetic approach for functional protein microarrays", *Anal. Biochem.* **2012**, *424*, 114-23.

(82) Chen, Y.; Muller, J. D.; Ruan, Q.; Gratton, E., "Molecular brightness characterization of EGFP in vivo by fluorescence fluctuation spectroscopy", *Biophys. J.* **2002**, *82*, 133-44.

(83) Cui, G.; Lan, Z.; Thiel, W., "Intramolecular hydrogen bonding plays a crucial role in the photophysics and photochemistry of the GFP chromophore", *J. Am. Chem. Soc.* **2012**, *134*, 1662-72.

(84) Wu, L.; Burgess, K., "Syntheses of highly fluorescent GFP-chromophore analogues", *J. Am. Chem. Soc.* **2008**, *130*, 4089-96.

(85) Conyard, J.; Kondo, M.; Heisler, I. A.; Jones, G.; Baldridge, A.; Tolbert, L. M.; Solntsev, K. M.; Meech, S. R., "Chemically modulating the photophysics of the GFP chromophore", *J. Phys. Chem. B.* **2011**, *115*, 1571-7.

(86) Ayyadurai, N.; Prabhu, N. S.; Deepankumar, K.; Jang, Y. J.; Chitrapriya, N.; Song, E.; Lee, N.; Kim, S. K.; Kim, B. G.; Soundrarajan, N.; Lee, S.; Cha, H. J.; Budisa, N.; Yun, H., "Bioconjugation of L-3,4-dihydroxyphenylalanine containing protein with a polysaccharide", *Bioconjug. Chem.* **2011**, *22*, 551-5.

(87) Kambe, N.; Iwasaki, T.; Terao, J., "Pd-catalyzed cross-coupling reactions of alkyl halides", *Chem. Soc. Rev.* **2011**, *40*, 4937-47.

(88) Taylor, R. H.; Felpin, F. X., "Suzuki-Miyaura reactions of arenediazonium salts catalyzed by PD(0)/C. One-pot chemoselective double cross-coupling reactions", *Org. Lett.* **2007**, *9*, 2911-4.

(89) Becht, J. M.; Catala, C.; Drian, C. L.; Wagner, A., "Synthesis of biaryls via decarboxylative Pd-catalyzed cross-coupling reaction", *Org. Lett.* **2007**, *9*, 1781-3.

(90) Felpin, F. X., "Practical and efficient Suzuki-Miyaura cross-coupling of 2-iodocycloenones with arylboronic acids catalyzed by recyclable Pd(0)/C", *J. Org. Chem.* **2005**, *70*, 8575-8.

(91) Kalia, J.; Raines, R. T., "Advances in Bioconjugation", *Curr. Org. Chem.* **2010**, *14*, 138-147.

(92) Nicolas, J.; Khoshdel, E.; Haddleton, D. M., "Bioconjugation onto biological surfaces with fluorescently labeled polymers", *Chem. Commun. (Camb)* **2007**, 1722-4.

(93) Burden, C. J.; Binder, H., "Physico-chemical modelling of target depletion during hybridization on oligonulceotide microarrays", *Phys. Biol.* **2010**, *7*, 016004.

(94) Liang, Y. Y.; Zhang, L. M., "Bioconjugation of papain on superparamagnetic nanoparticles decorated with carboxymethylated chitosan", *Biomacromolecules* **2007**, *8*, 1480-6.

(95) Hayashi, Y.; Yamaguchi, S.; Cha, W. Y.; Kim, D.; Shinokubo, H., "Synthesis of directly connected BODIPY oligomers through Suzuki-Miyaura coupling", *Org. Lett.* **2011**, *13*, 2992-5.

(96) Nemoto, H.; Cai, J.; Asao, N.; Iwamoto, S.; Yamamoto, Y., "Synthesis and biological properties of water-soluble p-boronophenylalanine derivatives. Relationship between water solubility, cytotoxicity, and cellular uptake", *J. Med. Chem.* **1995**, *38*, 1673-8.

(97) Capek, P.; Pohl, R.; Hocek, M., "Cross-coupling reactions of unprotected halopurine bases, nucleosides, nucleotides and nucleoside triphosphates with 4-boronophenylalanine in water. Synthesis of (purin-8-yl)- and (purin-6-yl)phenylalanines", *Org. Biomol. Chem.* **2006**, *4*, 2278-84.

(98) Amatore, C.; Le Duc, G.; Jutand, A., "Mechanism of palladium-catalyzed Suzuki-Miyaura reactions: multiple and antagonistic roles of anionic "bases" and their countercations", *Chemistry* **2013**, *19*, 10082-93.

(99) Bei, X.; Turner, H. W.; Weinberg, W. H.; Guram, A. S.; Petersen, J. L., "Palladium/P,O-ligand-catalyzed Suzuki cross-coupling reactions of arylboronic acids and aryl chlorides. Isolation and structural characterization of (P,O)-Pd(dba) complex", *J. Org. Chem.* **1999**, *64*, 6797-6803.

(100) Wang, Z. Y.; Ma, Q. N.; Li, R. H.; Shao, L. X., "Palladium-catalyzed Suzuki-Miyaura coupling of aryl sulfamates with arylboronic acids", *Org. Biomol. Chem.* **2013**, *11*, 7899-906.

Biographical Information

Yanbo Zhang received her Bachelor's degree in Biopharmaceutics in Huazhong University of Science and Technology in 2009. In 2009 she continued at the University of Texas at Arlington for her doctoral of philosophy in chemistry under the supervision of Dr. Roshan Perera. Her main project was based on bioengineering of heme proteins for biotechnology applications.